

RM-L50G19

RM L50G19

NACA RM L50G19

CASE FILE
COPY



NACA

RESEARCH MEMORANDUM

WIND-TUNNEL INVESTIGATION OF A NUMBER OF TOTAL-PRESSURE
TUBES AT HIGH ANGLES OF ATTACK

SUBSONIC SPEEDS

By William Gracey, William Letko, and Walter R. Russell

Langley Aeronautical Laboratory
Langley Air Force Base, Va.

JPL LIBRARY
CALIFORNIA INSTITUTE OF TECHNOLOGY

NATIONAL ADVISORY COMMITTEE
FOR AERONAUTICS

WASHINGTON

September 26, 1950

OCT 3 1950

NATIONAL ADVISORY COMMITTEE FOR AERONAUTICS

RESEARCH MEMORANDUM

WIND-TUNNEL INVESTIGATION OF A NUMBER OF TOTAL-PRESSURE
TUBES AT HIGH ANGLES OF ATTACK

SUBSONIC SPEEDS

By William Gracey, William Letko, and Walter R. Russell

SUMMARY

The National Advisory Committee for Aeronautics is investigating the possibility of developing a fixed total-pressure tube which will remain insensitive to inclination of the air stream over a wide range of angle of attack throughout the subsonic and supersonic speed ranges. As the first step in this program the variation of total-pressure error with angle of attack of 39 total-pressure tubes has been determined for an angle-of-attack range of $\pm 45^\circ$ and an indicated air speed of 195 miles per hour. The design of these tubes was varied in such a manner that the effects of external shape, internal shape, and configuration of the total-pressure entry could be determined. The external shapes tested included cylindrical, conical, and ogival nose sections. The internal shapes and total-pressure entries were varied on the basis of such factors as size of impact opening, shape of internal chamber, internal bevel, leading-edge sharpness, slant profile, and shielding (combined with venting).

The investigation showed that a shielded total-pressure tube (Kiel type) designed for end-mounting on a horizontal boom and having a vent area equal to 1.5 times the entrance area was the least sensitive to inclination of any of the tubes tested. The angle-of-attack range over which this tube remained insensitive to within 1 percent of the impact pressure was 41.5° .

A comparison of the calibrations of the remaining tubes showed that cylindrical tubes are less sensitive to misalignment than either conical or ogival nose sections. For simple straight-bore cylindrical tubes, it was shown that the range of insensitivity may be increased by increasing the size of the impact opening. For tubes having a very large bore extending 1 tube diameter behind the nose, the misalignment characteristics may be improved still further by the use of a hemispherical rather

than a cylindrical chamber. Cylindrical tubes incorporating a 15° internal bevel extending about 1.5 tube diameters to the rear of the nose were shown to provide even greater insensitivity to misalignment. An important feature of this tube was a sharp leading edge which was found to be generally effective in increasing the range of insensitivity of total-pressure tubes.

For airspeed applications where it is not essential that a tube be insensitive to large negative angles of attack, the range of insensitivity at positive angles of attack may be extended by the use of a slant profile. The range of insensitivity of a large-bore tube, for example, was shifted from $\pm 23^\circ$ to -13° and 32° by means of a 10° slant profile. The sensitivity of this tube at angles of yaw and at angles of attack combined with angles of yaw up to 15° was shown to be no greater than that of a similar tube having a straight leading-edge profile.

INTRODUCTION

With the development of high-speed airplanes having low-aspect-ratio wings and the capability of flying to high altitudes, it has become possible for airplanes to reach extremely high angles of attack at high speeds. Under these conditions the total pressure measured by a conventional fixed total-pressure tube may be appreciably in error because of the inclination of the tube to the air stream. Although these errors may be avoided by mounting the tube on pivots and adding vanes so that the tube will always align itself with the air stream, this type of tube is considered undesirable for high-speed flight because of the possible serious consequences of structural failure when the tube is mounted ahead of the fuselage nose.

In order to establish the optimum design of a fixed total-pressure tube for use at high angles of attack, the National Advisory Committee for Aeronautics has inaugurated a wind-tunnel program for investigating the characteristics of a number of total-pressure tubes through a large range of angle of attack in both the subsonic and supersonic speed ranges. This paper presents the results of the subsonic tests of the first group of tubes to be investigated. In the interest of early publication of the test results, the data are being presented at this time without detailed analysis.

SYMBOLS

- d diameter of impact opening of tube
D body diameter of tube

| | |
|------------|--|
| H | total pressure of free stream |
| H' | total pressure measured by tube |
| ΔH | H' - H |
| q_c | free-stream impact pressure |
| α | angle of attack of total-pressure tube |
| ψ | angle of yaw of total-pressure tube |

APPARATUS AND TESTS

The 39 total-pressure tubes which were tested during this investigation are shown in figures 1 to 5. (Design details and pertinent dimensions of each of the tubes are given in figs. 9 to 47.) With the exception of tubes A-10 to A-13 and E-1 the body diameter of all of the tubes was 1 inch.

For purposes of comparison the 39 tubes have been divided into five groups on the basis of the external shape of the nose sections - cylindrical (Series A), 15° conical (Series B), 30° conical (Series C), 45° conical (Series D), and ogival (Series E). The design of the various tubes in each of the five series was varied as regards both internal shape and configuration of total-pressure entry. It may be noted in figure 1 that tubes A-10 to A-13 were actually the same tube in which the number of exit orifices were increased on four successive tests. Similarly, tubes A-2 and A-3 were identical except for the thickness of the wall at the entry.

The tests were conducted in the 6- by 6-foot test section of the Langley stability tunnel. The tube support employed during these tests was a special U-shaped swivel mechanism (figs. 6 and 7) which was mounted on the side wall of the tunnel. This support was designed with the axis of rotation directly below the tip of the total-pressure tube in order that the total-pressure entry would remain at the same point in the air stream regardless of the angular setting of the tube. The inclination of the tube to the air flow was set by means of a control arm and angular scale on the outside of the tunnel wall (figs. 7 and 8). Possible errors caused by deflection of the support mechanism were investigated at an angular setting of 45° and were found to be negligible.

Each tube was tested at an impact pressure of 100 pounds per square foot or an indicated airspeed of about 195 miles per hour. At this speed the tube was rotated through an angular range of $\pm 45^\circ$ in 5° increments.

For each setting of the tube the total-pressure error was determined by measuring the pressure difference between the test tube and a fixed pitot-static tube mounted on the opposite side of the tunnel (fig. 6). The pitot-static tube was also used to provide a measure of the impact pressure at which the tests were conducted. The accuracy of the measurements of $\Delta H/q_c$ was estimated to be within 0.002.

RESULTS AND DISCUSSION

The results of the tests of the 39 total-pressure tubes are presented in figures 9 to 47. The symbol ΔH shown in these figures represents the total-pressure error, which is defined by the relation $H' - H$, where H' is the total pressure measured by the tube and H is free-stream total pressure. These total-pressure errors are presented as fractions of the impact pressure q_c and are plotted as a function of the angle of attack α (or angle of yaw ψ) of the tubes.

In the following discussion the calibrations of each series of tubes are treated separately in order to show the effects of internal shape and configuration of the total-pressure entry on the characteristics of a given external shape. At the end of this discussion the calibrations of comparable tubes in each of the five series are compared to show the effect of variations in external shape. The criterion which has been chosen for these comparisons is the range of angle of attack over which the tube remains insensitive to within 1 percent of the impact pressure. For convenience in making these comparisons the range of insensitivity of the 39 tubes has been summarized in table I.

Cylindrical tubes - Series A. - The calibrations of 13 total-pressure tubes having a straight external wall are presented in figures 19 to 21. The design of these tubes was varied in such a manner that the effects of size of impact opening, shape of internal chamber, slant of leading-edge profile, internal bevel, and shielding (combined with venting) might be investigated.

The variation of tube sensitivity with impact opening size (or more specifically, the ratio of impact opening diameter d to tube diameter D) may be determined by comparing figures 9 to 11. Examination of the two extreme cases, tubes A-1 and A-2, will show that the tube having the larger d/D ratio has the greater insensitivity to misalignment. For example, the range of insensitivity of the large-bore tube, A-2 ($\frac{d}{D} = 0.98$) is $\pm 23^\circ$, whereas that of the small-bore tube A-1 ($\frac{d}{D} = 0.125$) is only $\pm 11^\circ$. Small differences in impact opening size, on the other hand, have a negligible effect on the range of insensitivity of the tube. Figures 10 and 11 show that for a decrease in d/D from 0.98 (tube A-2) to 0.96

(tube A-3) the range of insensitivity is exactly the same. That the detrimental effect of the smaller impact opening is still present, however, is evident from the fact that the total-pressure error of tube A-3 at $\alpha = 45^\circ$ is slightly larger than that for tube A-2. These results are in general agreement with those reported in references 1 and 2 for hemispherical nosed tubes over a range of 24° .

The effect of the shape of the internal chamber on the characteristics of large-bore tubes having blunt leading edges is shown in figures 10 and 13. The design of these tubes was identical as regards the size of the impact opening and the depth of the chamber (1 tube diameter behind the nose). The chamber of tube A-2, however, was cylindrical while that for A-5 was hemispherical. Comparison of the calibrations of the two tubes will show that the performance of the tube is improved by changing the chamber from cylindrical to hemispherical and that the magnitude of this improvement is about $2\frac{1}{2}$.

The effect of internal shape on cylindrical tubes having sharp leading edges may be seen from a comparison of the calibrations of tubes A-4 and A-8 (figs. 12 and 16). These two tubes are alike in that both have 20° internally bevelled leading edges, but differ in that tube A-4 has a cylindrical chamber (1 diameter behind the nose) while tube A-8 has a 20° conical chamber. As indicated by figures 12 and 16 the conical chamber has a beneficial effect on the performance of the tube, for the range of insensitivity is about $2\frac{1}{2}$ greater than that of the tube with the cylindrical chamber. On the basis of this and the previous discussion of internal shape, it is apparent that both conical and hemispherical chambers are superior to cylindrical chambers.

The effect of varying the slant of the leading-edge profile of a cylindrical tube is shown in figures 10 and 14(a). Changing the profile from square (tube A-2) to a slant of 10° (tube A-6) is shown to have a beneficial effect in shifting the curve by about 10° so that the tube remains insensitive to higher positive angles of attack. The range of insensitivity of tube A-6, for example, extends from -13° to 32° , whereas that of tube A-2 is only $\pm 23^\circ$. The sensitivity of tube A-6 to angle of yaw is presented in figure 14(b). As shown by this figure the range of insensitivity is $\pm 23^\circ$, which is the same as that for tube A-2. The characteristics of tube A-6 at angles of yaw combined with angles of attack are given in figure 14(c). The curves on this figure show that the range of angle of attack over which the tubes remain insensitive decreases progressively as the angle of yaw is increased to 20° . For angles of yaw as high as 15° , however, the tube is still insensitive to within 1 percent q_c for an angle-of-attack range of -9° to 23° . It may be concluded, therefore, that a slant profile of 10° has the effect of improving the characteristics of the tube for positive angles of attack ($\psi = 0^\circ$) without loss in performance

at either angles of yaw ($\alpha = 0^\circ$) or angles of attack combined with angles of yaw up to 15° .

The misalignment characteristics of straight-walled tubes having internal bevels of 15° , 20° , and 25° are shown in figures 15 to 17. These figures show the range of insensitivity of the tube to increase progressively as the bevel angles is decreased. For an internal bevel of 15° the tube is insensitive over a range of $\pm 27.5^\circ$, whereas for a bevel angle of 25° the range of insensitivity is only $\pm 23.5^\circ$.

The calibrations of shielded total-pressure tubes having vent areas varying from 0 to 1.5 times the entrance area are shown in figures 18 to 21. The design of these tubes was based on that of the Kiel shielded total-pressure tube reported in reference 3. The present design differs from the Kiel tube, however, in the type of mounting attachment, for the Kiel tube was fitted with a transverse spindle whereas the present tube was designed for end-mounting on a horizontal boom. This feature was incorporated in the present design in order to avoid the vibrational difficulties which have been encountered at high speeds with spindle-mounted tubes. The calibrations in figures 18 and 19 show that the effect of venting a shielded tube is considerable. The range of insensitivity of the unvented tube A-10, for example, is $\pm 24^\circ$ whereas that of the tube having a vent area equal to one-half the entrance area is $\pm 38.5^\circ$. Increasing the vent area to 1 and 1.5 times the entrance area extends the range of insensitivity of the tube to 41° and 41.5° , respectively. (See figs. 20 and 21.) It may be noted at this point that the range of insensitivity of tube A-13 was the largest of any of the 39 tubes tested during this investigation.

Conical tubes - series B, C, and D. - The misalignment characteristics of conical nose tubes having external bevel or cone angles of 15° , 30° , and 45° (series B, C, and D, respectively) are given in figures 22 to 41. The design factors which were studied with these tubes included leading-edge sharpness, impact-opening size, and internal bevel.

The effect of leading-edge sharpness on conical-nose tubes may be determined by comparison of the calibrations of tubes B-1, B-2, and B-3; C-1, C-2, and C-3; and D-1, D-2, and D-3. (See figs. 22 to 24, 28 to 30, and 36 to 38.) The impact opening of each of these tubes was $\frac{1}{8}$ -inch diameter and the wall thickness at the impact opening for each of the three series of tubes was varied from 0 to 0.05 to 0.10 inch. For the conical-nose tube of 15° , the range of insensitivity was decreased from 21° to 13° to 10.5° as the leading-edge sharpness was decreased by the amounts noted (figs. 22 to 24). Figures 28 to 30 and 36 to 38 show that the range of insensitivity of tubes having cone angles of 30° and 45°

varies in a similar manner. It will be noted, however, that the total-pressure errors of the blunt-nose tubes having cone angles of 30° and 45° are smaller than those of the sharp-nose tubes at the higher angles of attack.

The effect of impact opening size on the characteristics of a conical-nose tube of 30° are shown in figures 28, 31, and 32. These figures show that for an increase in the size of the impact opening from $1/16$ to $1/8$ to $3/16$ inch, the range of insensitivity of the tube is increased from 15.5° to 17.5° to 19° , respectively. These results are similar to those obtained with cylindrical tubes in showing the advantage of large d/D ratios.

The characteristics of conical-nose sections having internally beveled total-pressure entries may be shown by comparing the calibrations of tubes B-4, B-5, and B-6; C-6, C-7, and C-8; and D-4, D-5, and D-6 (figs. 25 to 27, 33 to 35, and 39 to 41). These curves show that for each of the three cone angles the tubes having an internal bevel of 15° are less sensitive to misalignment than tubes having 20° and 25° bevels. It will be recalled that this variation of tube sensitivity with internal bevel angle is the same as that shown for internal bevels on cylindrical tubes.

Ogival tubes - series E. - Calibrations of total-pressure tubes having a nose section similar to that of the Kollsman type 651-B pitot-static tube are presented in figures 42 to 47. The total-pressure entries of these tubes were varied on the basis of leading-edge sharpness, profile slant, and internal bevel.

Tube E-1 was an actual Kollsman tube ($\frac{29}{32}$ -inch-body diameter) which was adapted for mounting on the swivel test rig used in this investigation. The total-pressure entry of this tube was reworked for these tests to a sharp leading edge by reaming the impact opening to a diameter of 0.29 inch. The nose shape of the remaining tubes was patterned after that of the Kollsman tube except that the body diameter for these tubes was 1 inch.

An approximate indication of the effectiveness of sharpening the leading edge of this type tube may be obtained by comparing the tests of tubes E-1 and E-2 (figs. 42 and 43). The sharp-edged entry remained insensitive over a range of angle of attack of $\pm 16^\circ$, whereas the blunt-nosed tube was insensitive from only -1.5° to 11.5° . The asymmetry of the curve for the second tube is, of course, due to the 10° oblique profile. If the forward profile of this tube had been straight, the curve would presumably have been symmetrical about zero angle of attack and the tube insensitive over a range of $\pm 6.5^\circ$.

The effect of changing the slant of the leading-edge profile from 10° to 20° is shown in figures 43 and 44. These curves show that whereas tube E-2 is insensitive over an angle-of-attack range of from -1.5° to 11.5° tube E-3 is insensitive from 8.5° to 21.5° . In other words, the effect of increasing the slant angle from 10° to 20° is a shift of the curve on the angle-of-attack scale of 10° .

The effect of varying the internal bevel from 15° to 25° on an ogival-shaped tube is shown in figures 45 to 47. As shown by these figures, the range of insensitivity decreases from 19° to 18.5° to 18° as the bevel angle increases from 15° to 20° to 25° . The variation of tube sensitivity with bevel angle is, therefore, the same as that for cylindrical and conical nose tubes. The magnitude of the variation, however, for equal changes in bevel angles is somewhat less than that for the cylindrical and conical tubes.

An interesting phenomenon which was encountered during these tests is that at high angles of attack the indications of some of these tubes became very erratic and that these irregularities were accompanied by a loud whistling sound which could be heard through the walls of the tunnel. When tube E-1, for example, was moved through the angle-of-attack range, the indicated pressures would sometimes follow the solid line shown in figure 42 and for this case no whistling could be discerned. During other tests, however, the indicated pressures would follow the dashed curve (that is, the total-pressure errors were increased) and under these conditions the tube whistled as indicated above. The exact cause of this effect is not entirely clear, for it was noted during the tests of tubes E-1 and E-3 but not of tube E-2 (which had a chamber of the same size and shape as that of E-3 and differed only in the obliqueness of the profile). With tube E-1 the effect began at angles of attack of $\pm 40^\circ$. With E-3 the whistling began at -25° which, when added to the effective zero (15°) of this tube, is also equivalent to 40° . These acoustic effects may be eliminated by decreasing the length of the internal chamber, but just what the critical length is for chambers of this shape was not determined during this investigation.

External shape - series A, B, C, D, and E. - The effect of external shape on the misalignment characteristics of total-pressure tubes can be determined by comparing tubes having the same type of total-pressure entry in each of the five series. For example, comparison of tubes having an internal bevel of 20° (figs. 16, 26, 34, 40, and 46) will show that the range of insensitivity of the tubes having a straight external wall is greater than that of the tubes having conical and ogival nose sections. The range of insensitivity of the 15° conical tube, in turn, is greater than that of the conical tubes of 30° and 45° and is about the same as that for the ogival tube. Similar trends may be noted from comparison of tubes which have other types of entry.

CONCLUDING REMARKS

The more significant conclusions which may be drawn from the results of subsonic tests of the total-pressure errors of 39 total-pressure tubes over an angle-of-attack range of $\pm 45^\circ$ are summarized below.

A shielded total-pressure tube (Kiel type) designed for end-mounting on a horizontal boom and having a vent area equal to 1.5 times the entrance area exhibited the least sensitivity to inclination of any of the tubes tested. The angle-of-attack range over which this tube remained insensitive to within 1 percent of the impact pressure was 41.5° .

From the standpoint of the various design factors which were studied during the investigation, the following results appear noteworthy. Tubes having a cylindrical external shape are less sensitive to misalignment than tubes having conical or ogival nose sections. For simple, straight-bore cylindrical tubes, the range of insensitivity may be increased by increasing the relative size of the impact opening. For tubes having a very large bore extending 1 tube diameter behind the nose, the misalignment characteristics may be improved still further by the use of a hemispherical rather than a cylindrical chamber. Cylindrical tubes incorporating a 15° internal bevel extending about 1.5 tube diameters to the rear of the nose provide even greater insensitivity to misalignment. An important feature of this tube was a sharp leading edge, which was found to be generally effective in increasing the range of insensitivity of total-pressure tubes.

For airspeed applications where it is not essential that a tube be insensitive to large negative angles of attack, the range of insensitivity at positive angles of attack may be extended by the use of a slant profile. The range of insensitivity of a large-bore tube, for example, was increased from 23° to 31.5° by means of a slant profile of 10° . The sensitivity of this tube to angles of yaw and to angles of attack combined with angles of yaw up to 15° was no greater than that of a similar tube having a straight-leading-edge profile.

Langley Aeronautical Laboratory
National Advisory Committee for Aeronautics
Langley Air Force Base, Va.

REFERENCES

1. Merriam, Kenneth G., and Spaulding, Ellis R.: Comparative Tests of Pitot-Static Tubes. NACA TN 546, 1935.
2. Huston, Wilber B.: Accuracy of Airspeed Measurements and Flight Calibration Procedures. NACA Rep. 919, 1948.
3. Kiel, G.: Total-Head Meter with Small Sensitivity to Yaw. NACA TM 775, 1935.

TABLE I.- ANGULAR RANGE OVER WHICH TOTAL-PRESSURE TUBES ARE INSENSITIVE TO MISALIGNMENT TO WITHIN 1 PERCENT OF IMPACT PRESSURE

| Tube | Figure | External shape | Internal shape | Total-head entry | Range of insensitivity (deg) |
|------|--------|----------------|---|-------------------------------|------------------------------|
| A-1 | 9 | Cylindrical | ----- | $\frac{d}{D} = 0.125$ - blunt | $\alpha = \pm 11$ |
| 2 | 10 | ----do---- | Cylindrical chamber | $\frac{d}{D} = 0.98$ - blunt | $\alpha = \pm 23$ |
| 3 | 11 | ----do---- | -----do----- | $\frac{d}{D} = 0.96$ - blunt | $\alpha = \pm 23$ |
| 4 | 12 | ----do---- | -----do----- | 20° internal bevel | $\alpha = \pm 23$ |
| 5 | 13 | ----do---- | Hemispherical chamber | $\frac{d}{D} = 0.98$ - blunt | $\alpha = \pm 25.5$ |
| 6 | 14(a) | ----do---- | Cylindrical chamber | $\frac{d}{D} = 0.98$ - blunt | $\alpha = -13 + 32$ |
| 6 | 14(b) | ----do---- | -----do----- | 10° slant profile | $\psi = \pm 23$ |
| 7 | 15 | ----do---- | 15° internal bevel | Sharp | $\alpha = \pm 27.5$ |
| 8 | 16 | ----do---- | 20° internal bevel | --do- | $\alpha = \pm 25.5$ |
| 9 | 17 | ----do---- | 25° internal bevel | --do- | $\alpha = \pm 23.5$ |
| 10 | 18 | ----do---- | Shielded unvented | ----- | $\alpha = \pm 24$ |
| 11 | 19 | ----do---- | Shielded vented ($\frac{1}{2}$ × frontal area) | ----- | $\alpha = \pm 38.5$ |
| 12 | 20 | ----do---- | Shielded vented (1 × frontal area) | ----- | $\alpha = \pm 41$ |
| 13 | 21 | ----do---- | Shielded vented ($1\frac{1}{2}$ × frontal area) | ----- | $\alpha = \pm 41.5$ |
| B-1 | 22 | 15° cone | ----- | Sharp | $\alpha = \pm 21$ |
| 2 | 23 | ----do---- | ----- | Blunt - 0.05 inch wall | $\alpha = \pm 13$ |
| 3 | 24 | ----do---- | ----- | Blunt - 0.10 inch wall | $\alpha = \pm 10.5$ |
| 4 | 25 | ----do---- | 15° internal bevel | Sharp | $\alpha = \pm 21$ |
| 5 | 26 | ----do---- | 20° internal bevel | --do- | $\alpha = \pm 19$ |
| 6 | 27 | ----do---- | 25° internal bevel | --do- | $\alpha = \pm 18$ |
| C-1 | 28 | 30° cone | ----- | Sharp - 1/8 inch orifice | $\alpha = \pm 17.5$ |
| 2 | 29 | ----do---- | ----- | Blunt - 0.05 inch wall | $\alpha = \pm 10.5$ |
| 3 | 30 | ----do---- | ----- | Blunt - 0.10 inch wall | $\alpha = \pm 9$ |
| 4 | 31 | ----do---- | ----- | Sharp - 1/16 inch orifice | $\alpha = \pm 15.5$ |
| 5 | 32 | ----do---- | ----- | Sharp - 3/16 inch orifice | $\alpha = \pm 19$ |
| 6 | 33 | ----do---- | 15° internal bevel | Sharp | $\alpha = \pm 20.5$ |
| 7 | 34 | ----do---- | 20° internal bevel | --do- | $\alpha = \pm 18$ |
| 8 | 35 | ----do---- | 25° internal bevel | --do- | $\alpha = \pm 17.5$ |
| D-1 | 36 | 45° cone | ----- | --do- | $\alpha = \pm 14$ |
| 2 | 37 | ----do---- | ----- | Blunt - 0.05 inch wall | $\alpha = \pm 9.5$ |
| 3 | 38 | ----do---- | ----- | Blunt - 0.10 inch wall | $\alpha = \pm 8.0$ |
| 4 | 39 | ----do---- | 15° internal bevel | Sharp | $\alpha = \pm 15.5$ |
| 5 | 40 | ----do---- | 20° internal bevel | --do- | $\alpha = \pm 15$ |
| 6 | 41 | ----do---- | 25° internal bevel | --do- | $\alpha = \pm 13.5$ |
| E-1 | 42 | Ogival | Ogival chamber | --do- | $\alpha = \pm 16$ |
| 2 | 43 | ----do---- | Ogival chamber | Blunt - 10° slant profile | $\alpha = -1.5 + 11.5$ |
| 3 | 44 | ----do---- | Ogival chamber | Blunt - 20° slant profile | $\alpha = -8.5 + 21.5$ |
| 4 | 45 | ----do---- | 15° internal bevel | Sharp | $\alpha = \pm 19$ |
| 5 | 46 | ----do---- | 20° internal bevel | --do- | $\alpha = \pm 18.5$ |
| 6 | 47 | ----do---- | 25° internal bevel | --do- | $\alpha = \pm 18$ |



Page intentionally left blank

Page intentionally left blank

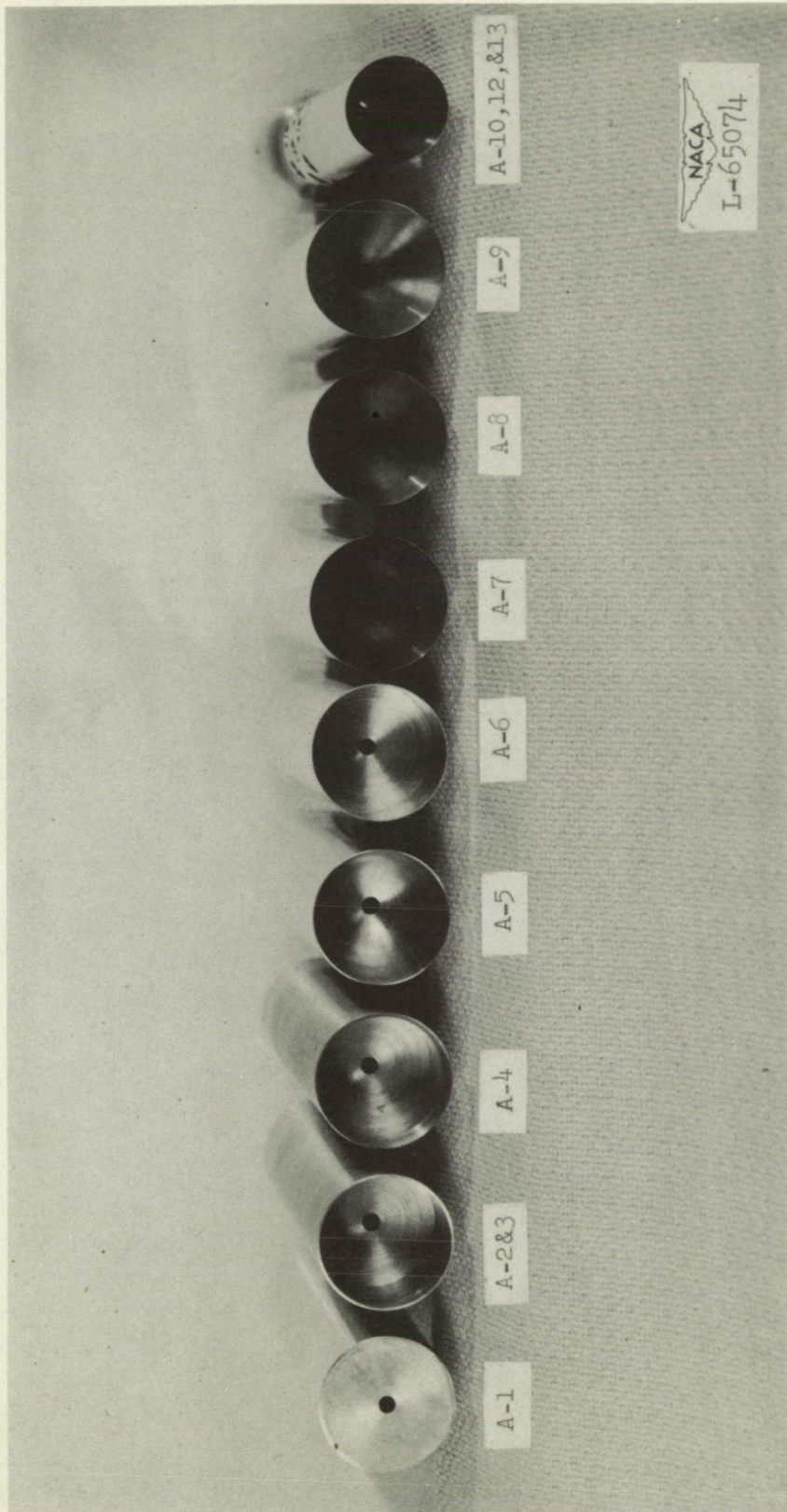


Figure 1.-- Total-pressure tubes having straight external wall. Series A.

Page intentionally left blank

Page intentionally left blank

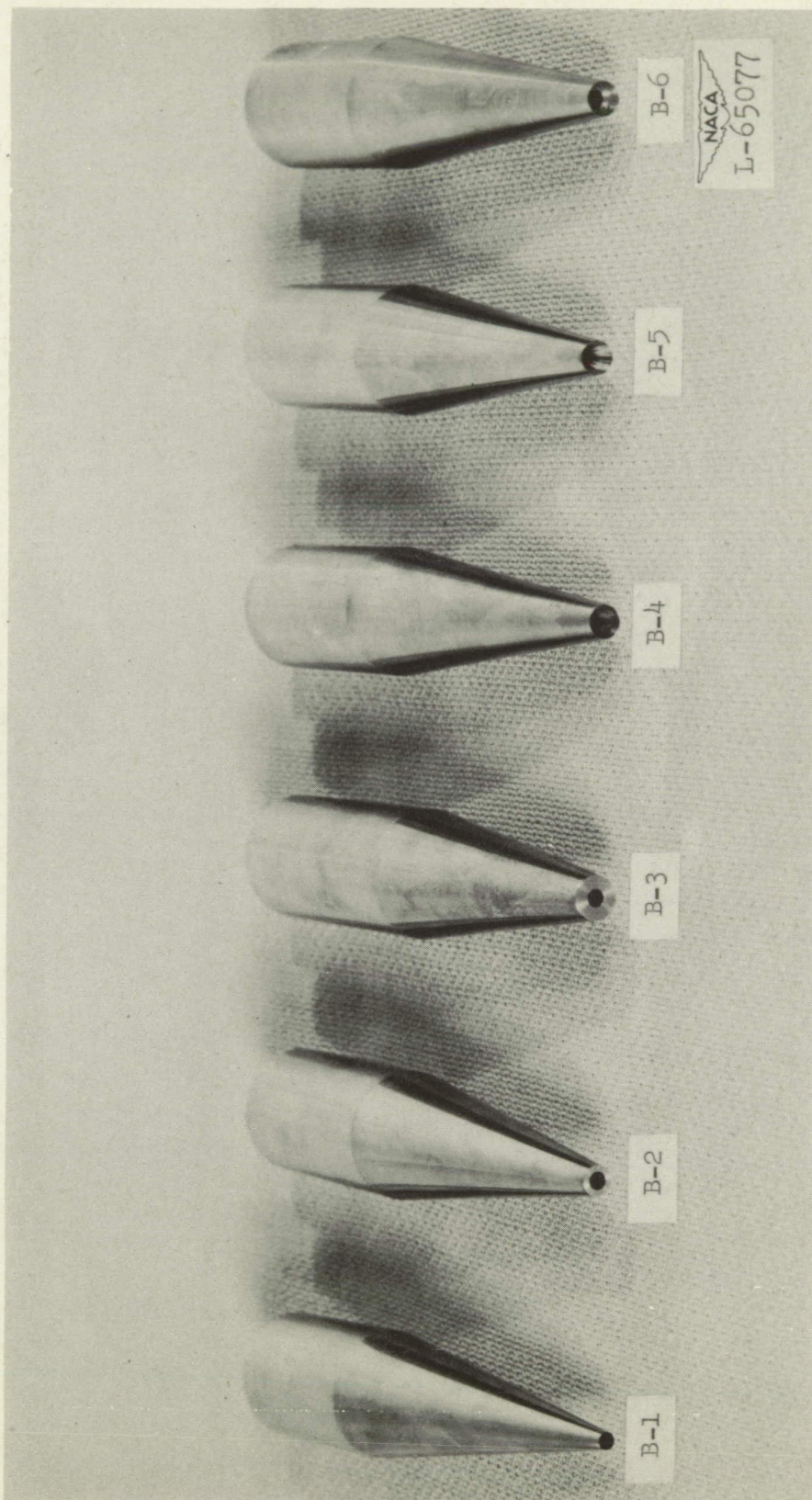


Figure 2.- Total-pressure tubes having 15° conical nose section. Series B.

Page intentionally left blank

Page intentionally left blank

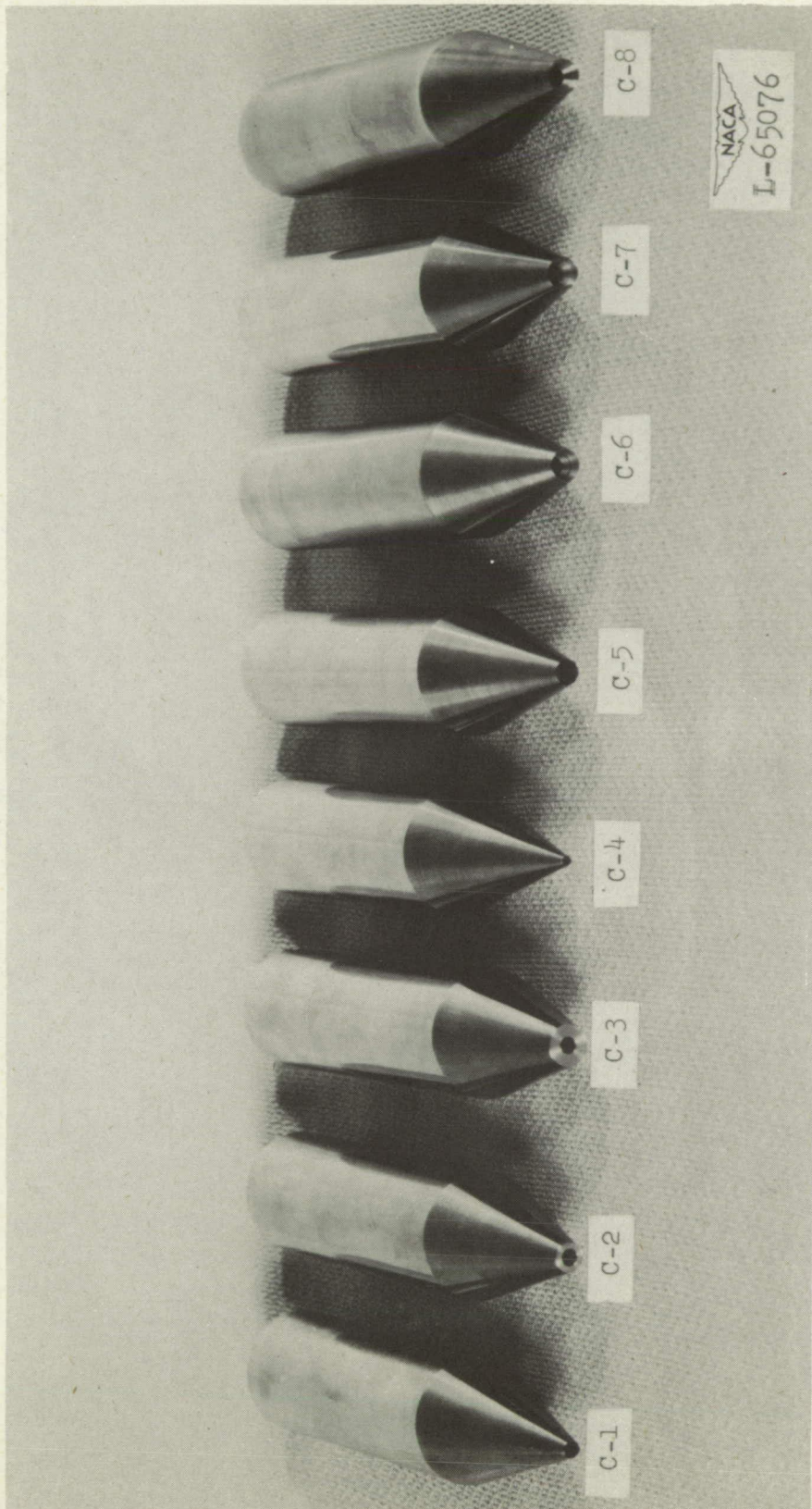


Figure 3.- Total-pressure tubes having 30° conical nose section. Series C.

Page intentionally left blank

Page intentionally left blank

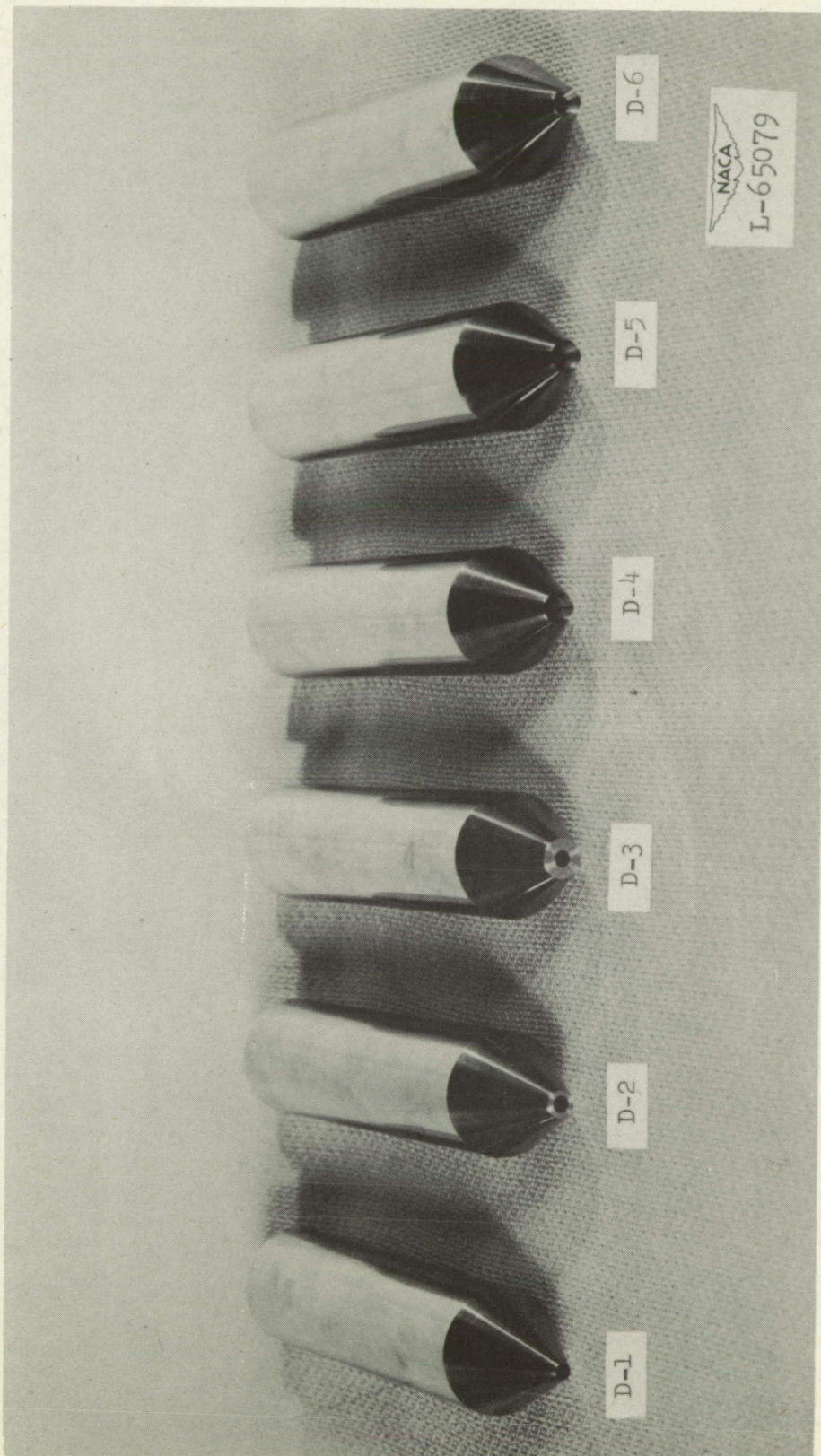


Figure 4.- Total-pressure tubes having 45° conical nose section. Series D.

Page intentionally left blank

Page intentionally left blank

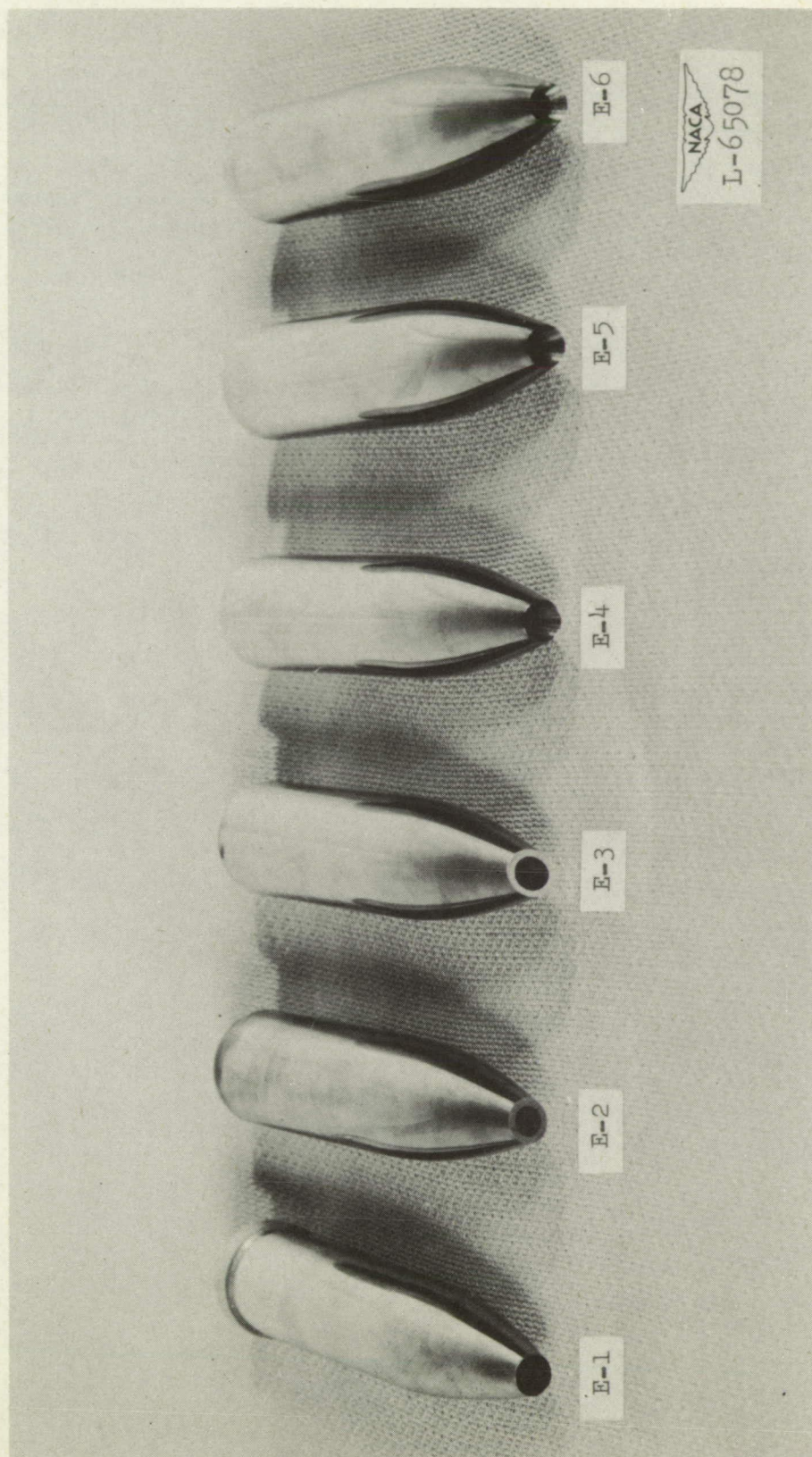


Figure 5.- Total-pressure tubes having ogival shaped nose section. Series E.

Page intentionally left blank

Page intentionally left blank



Figure 6.- View of Langley stability tunnel showing swivel arm with sample total-pressure tube on left wall and reference pitot-static tube on right wall.

Page intentionally left blank

Page intentionally left blank

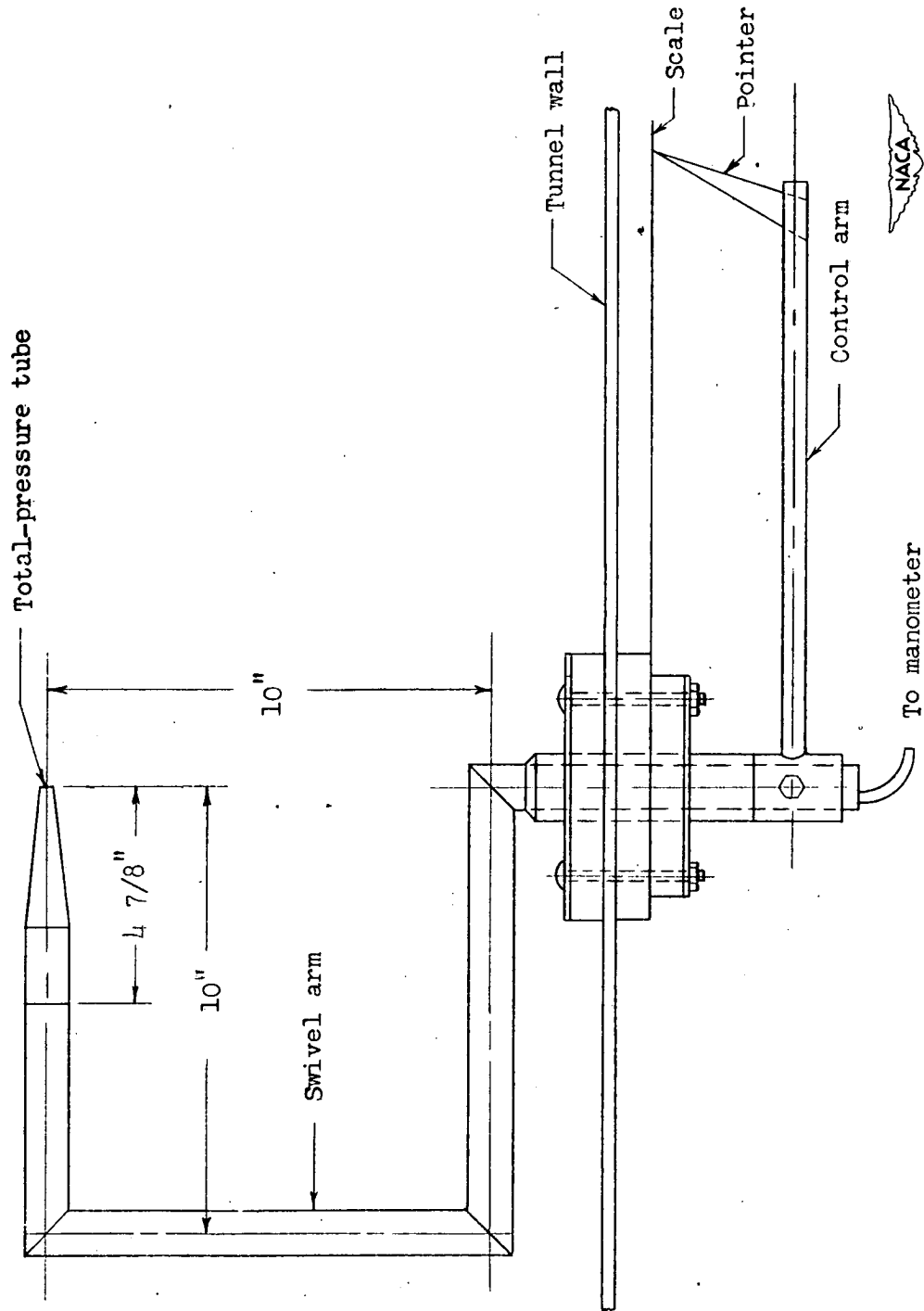


Figure 7.- Diagram of swivel mechanism used for changing angle of attack of total-pressure tubes.

Page intentionally left blank

Page intentionally left blank



Figure 8.- View outside of tunnel wall showing control arm, pointer, and angle-of-attack scale.

Page intentionally left blank

Page intentionally left blank

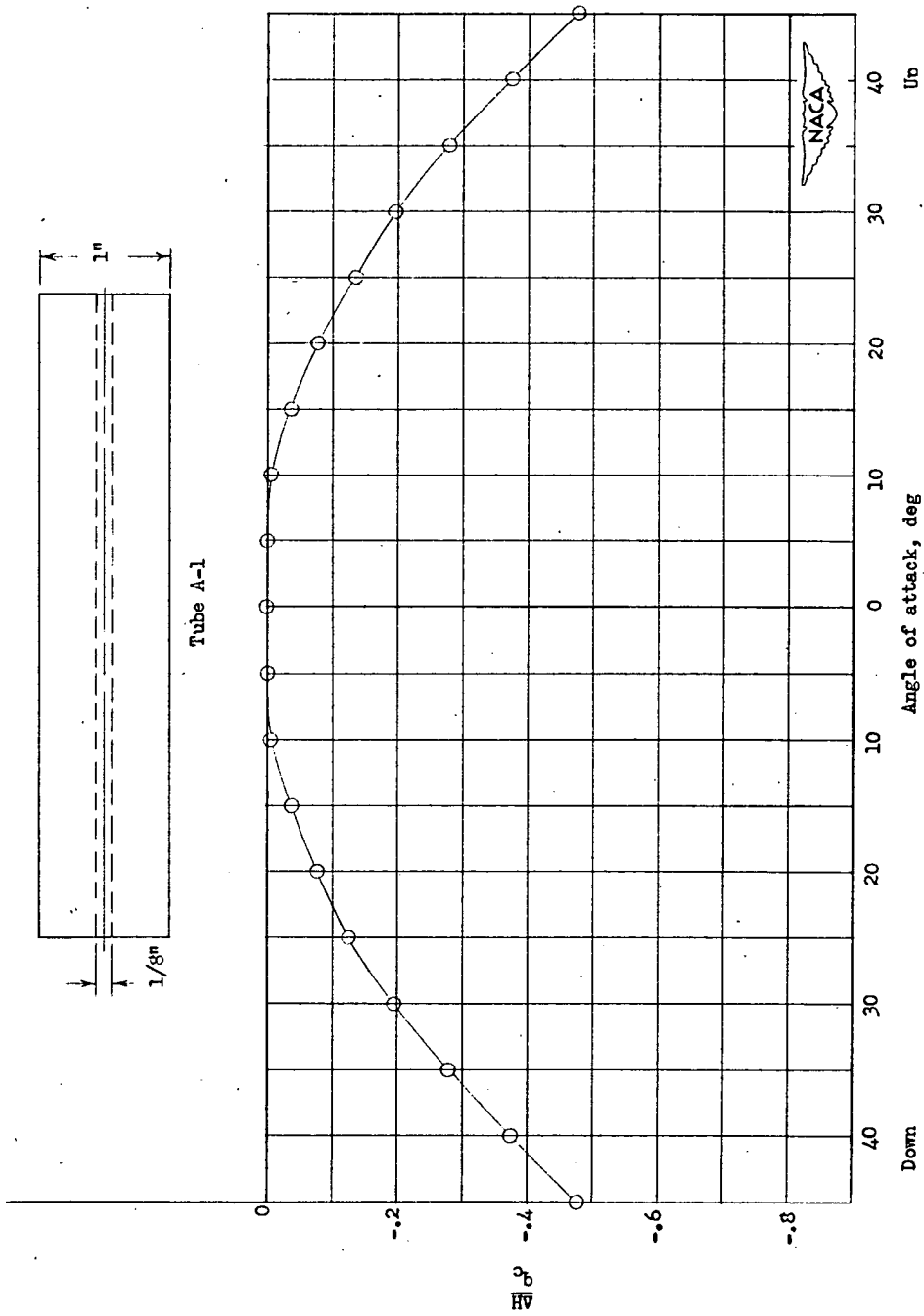


Figure 9.- Variation of total-pressure error with angle of attack.
Tube A-1.

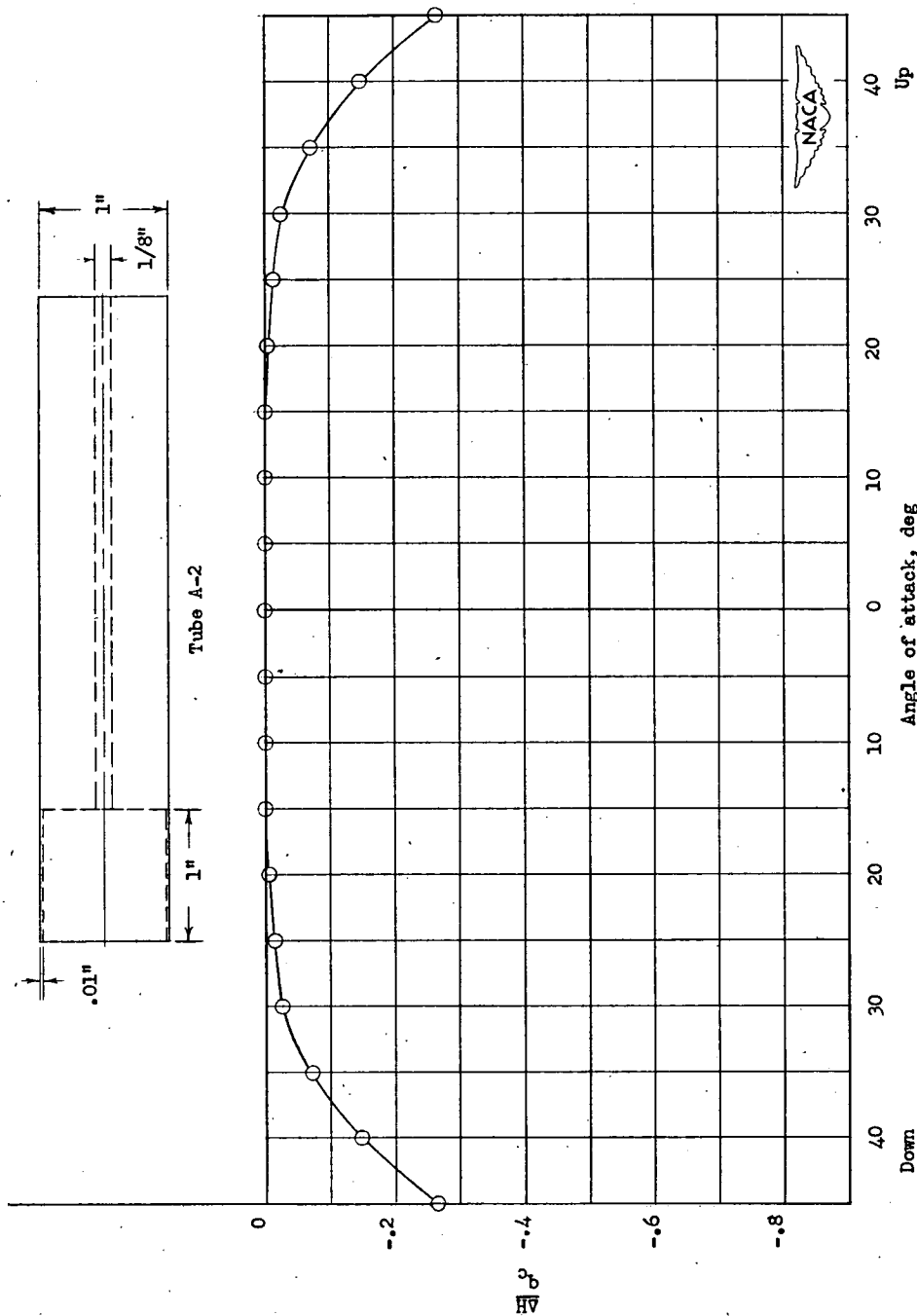


Figure 10.- Variation of total-pressure error with angle of attack.
Tube A-2.



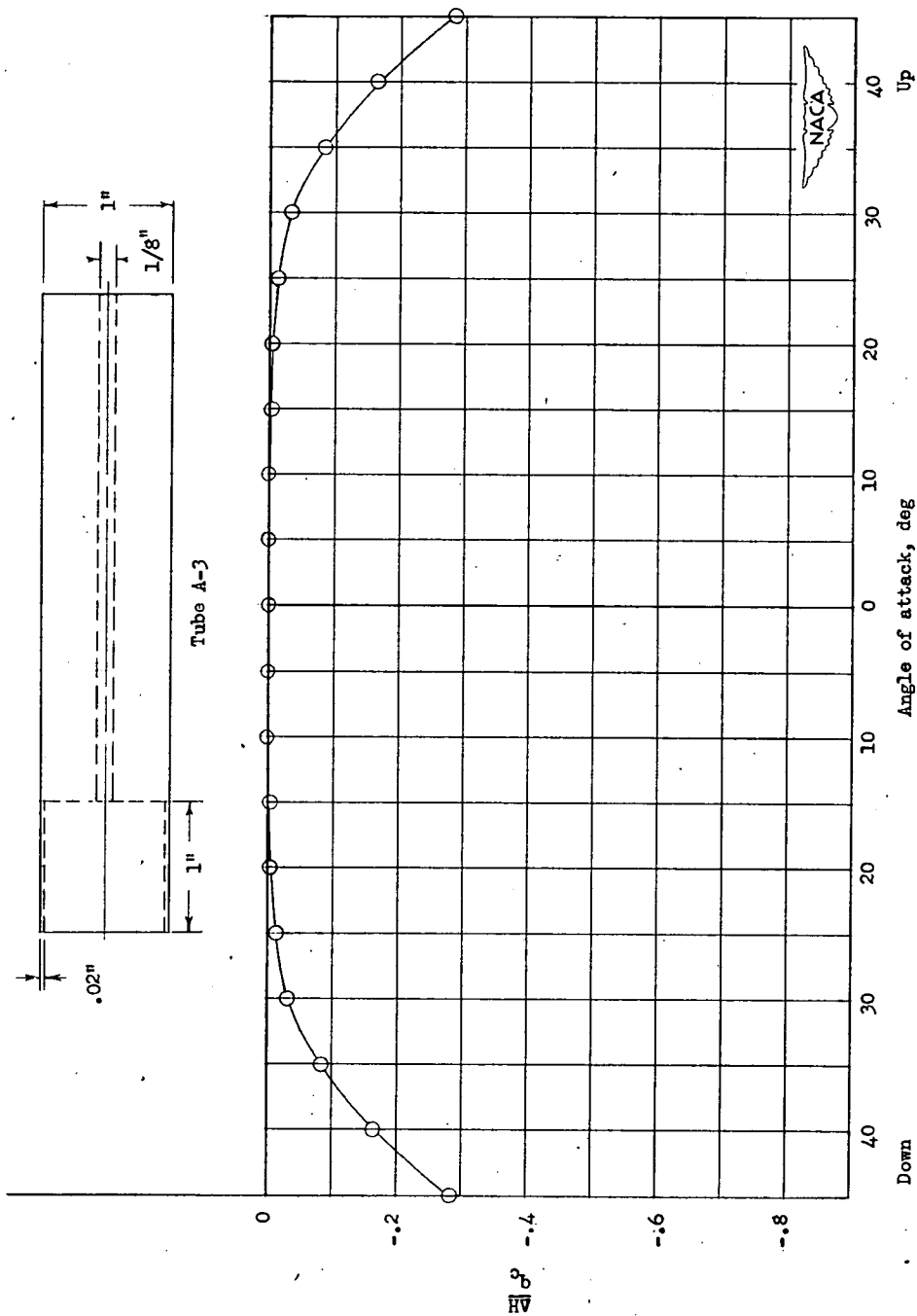


Figure 11.- Variation of total-pressure error with angle of attack. Tube A-3.

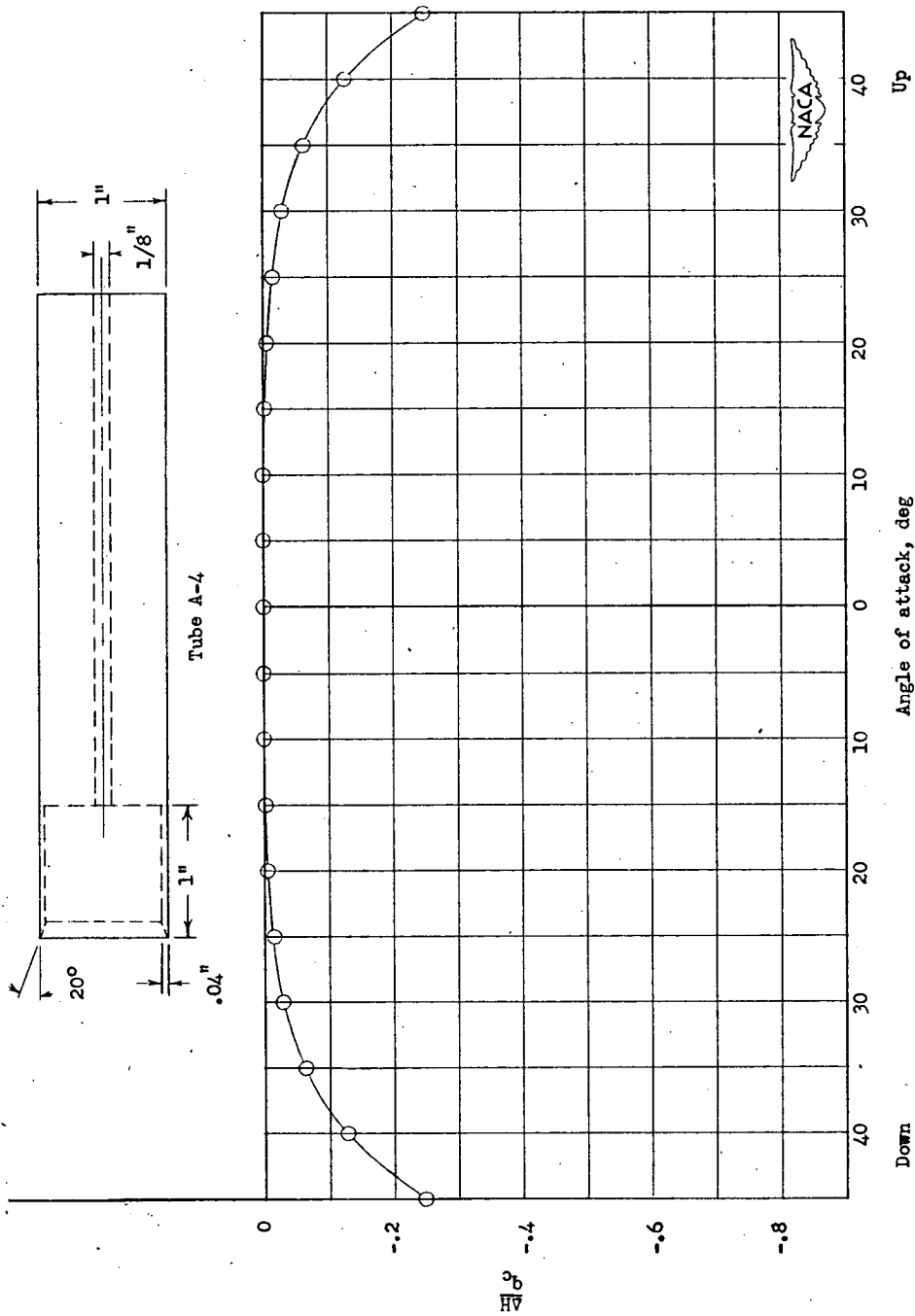


Figure 12.- Variation of total-pressure error with angle of attack. Tube A-4.

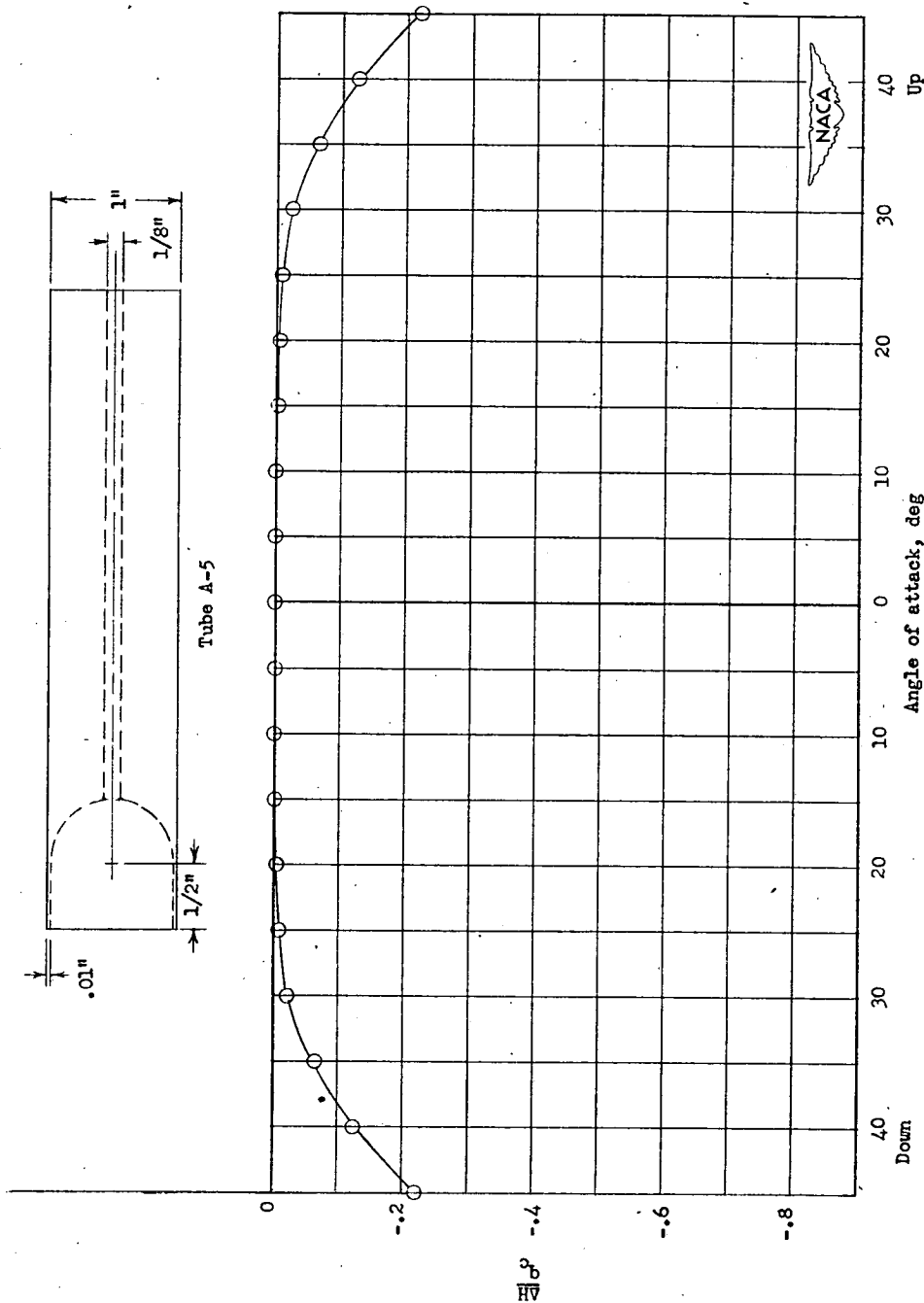
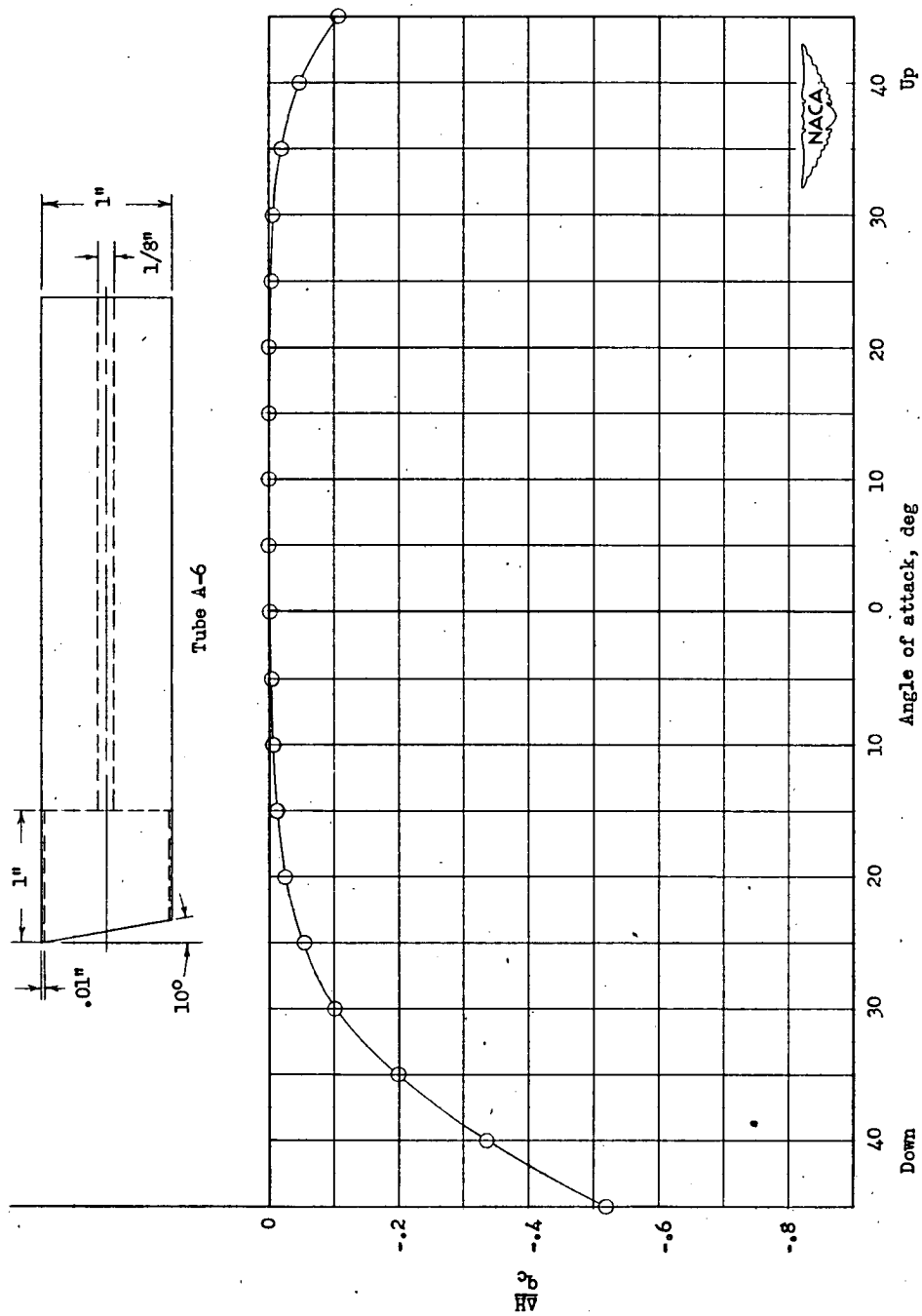
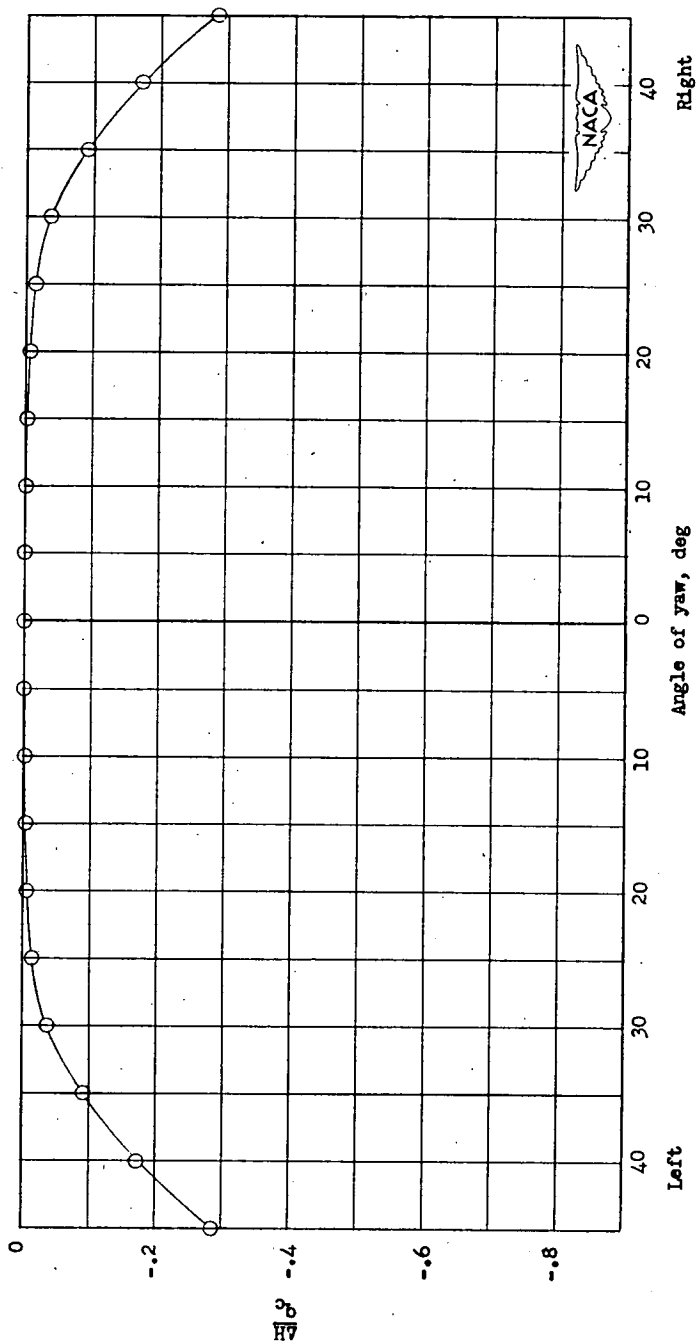


Figure 13.- Variation of total-pressure error with angle of attack.
Tube A-5.

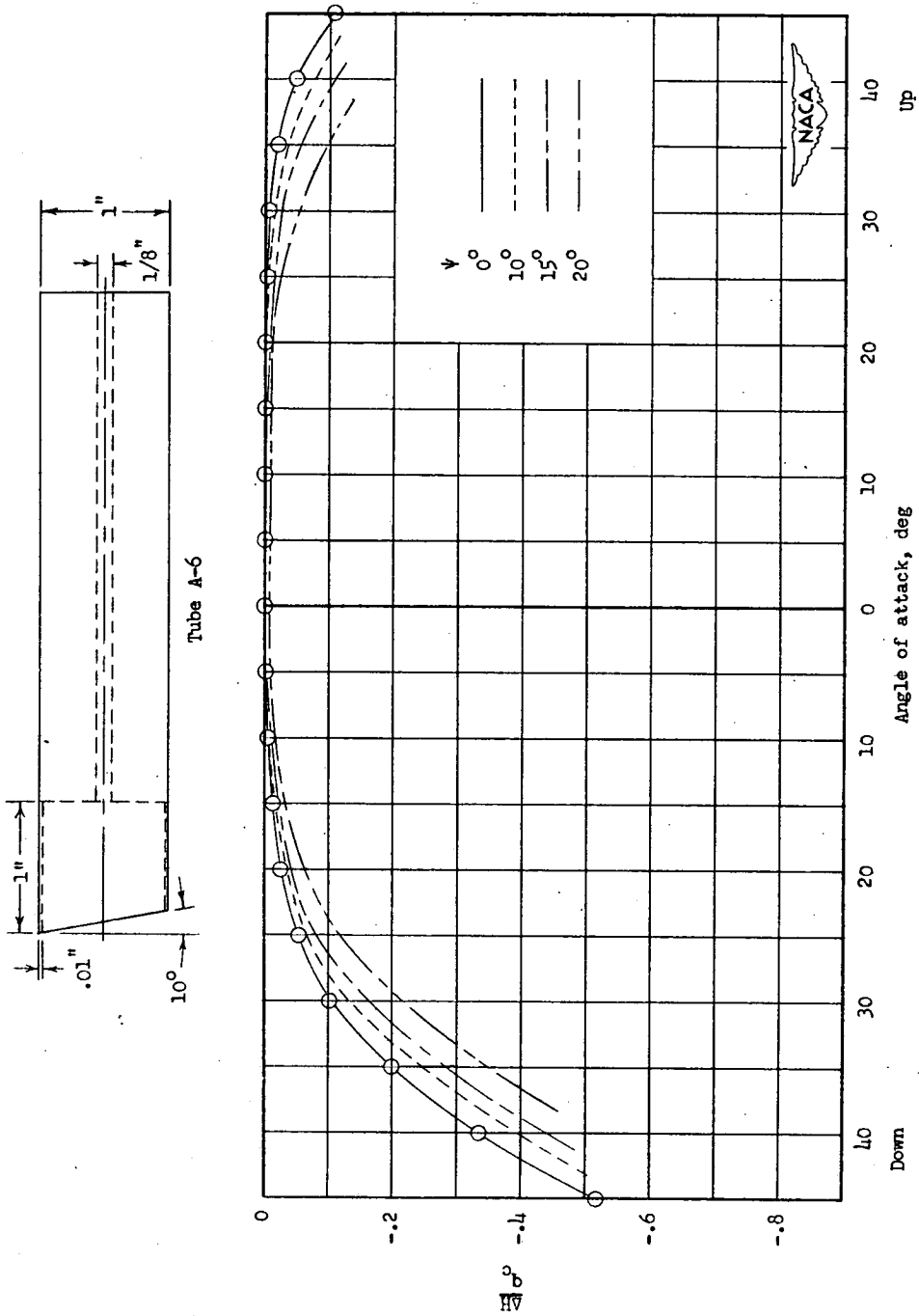


(a) Angle of attack ($\psi = 0$).
 Figure 14.- Variation of total-pressure error with inclination to the air stream. Tube A-6.



(b) Angle of yaw ($\alpha = 0$).

Figure 14.- Continued.



(c) Angles of attack combined with angles of yaw.

Figure 14.- Concluded.

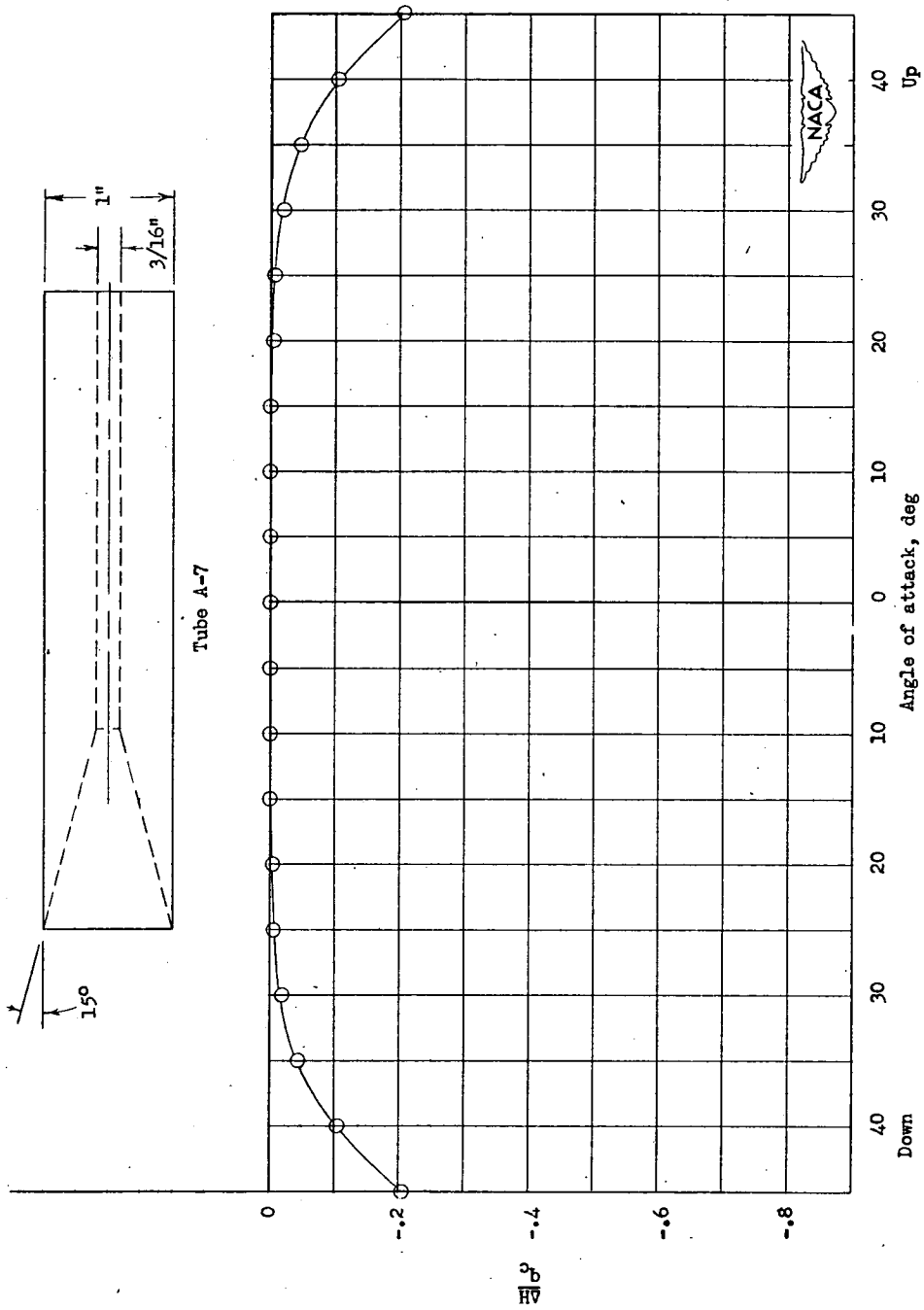


Figure 15 - Variation of total-pressure error with angle of attack. Tube A-7.

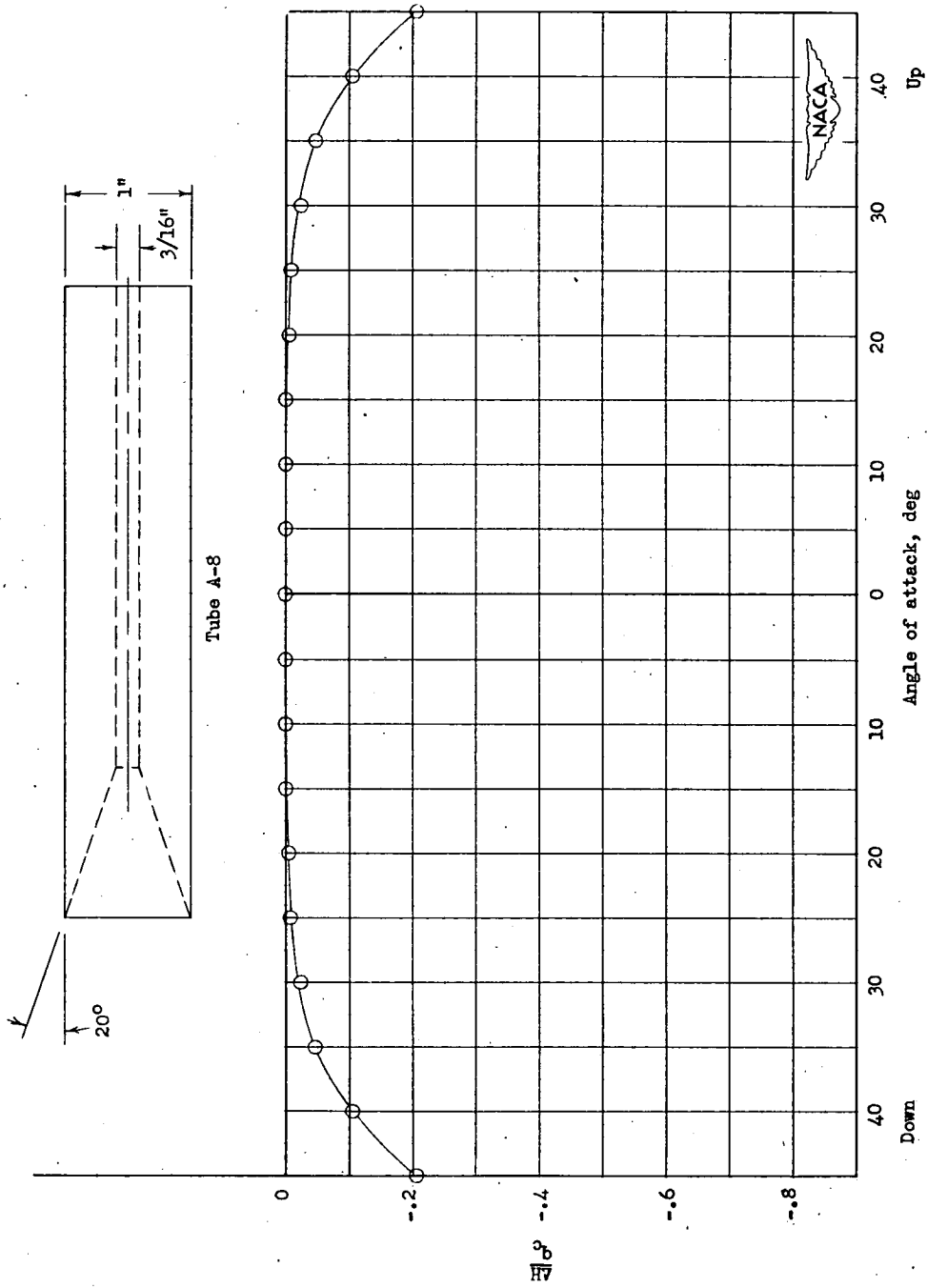


Figure 16.- Variation of total-pressure error with angle of attack. Tube A-8.

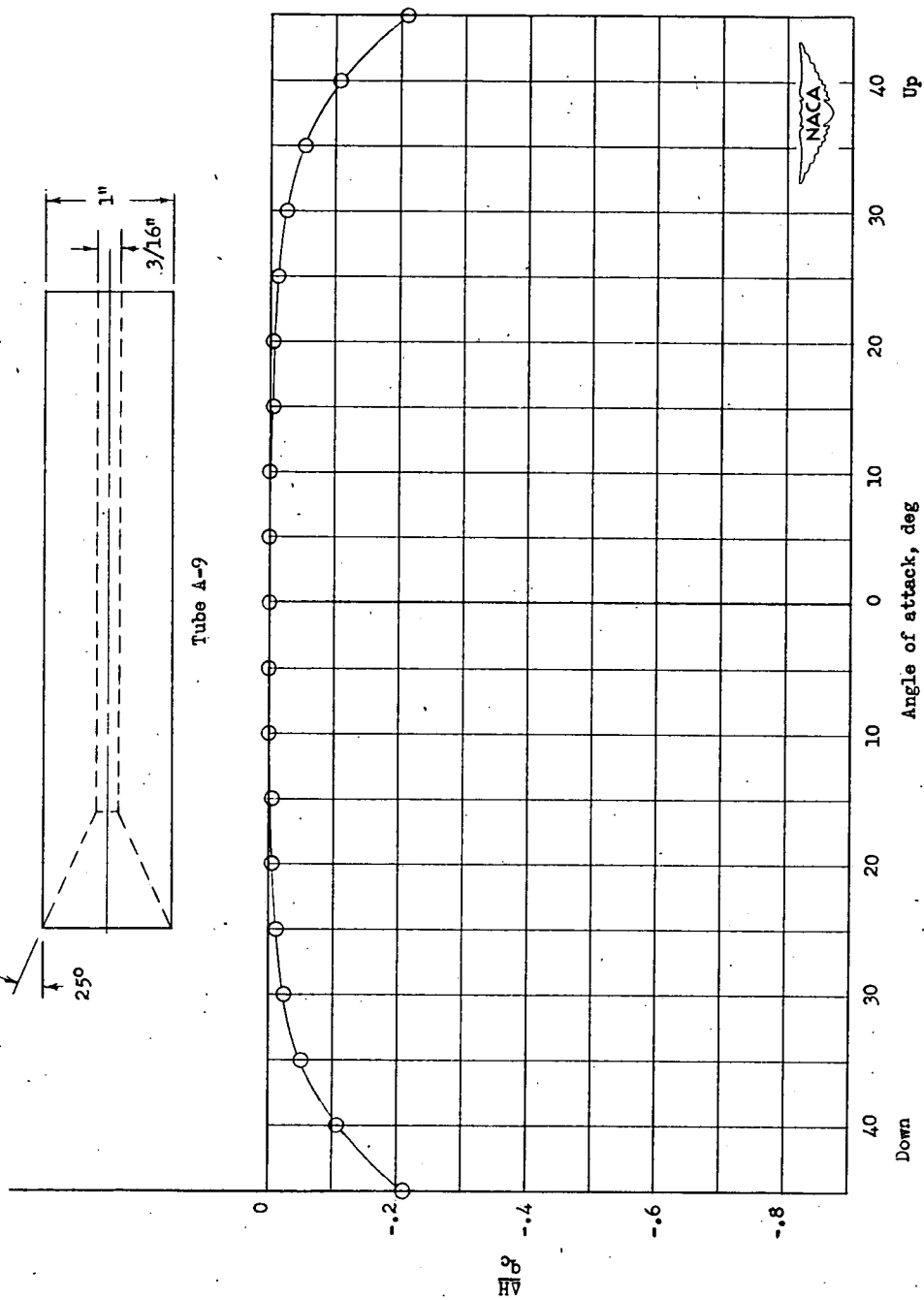


Figure 17.- Variation of total-pressure error with angle of attack. Tube A-9.

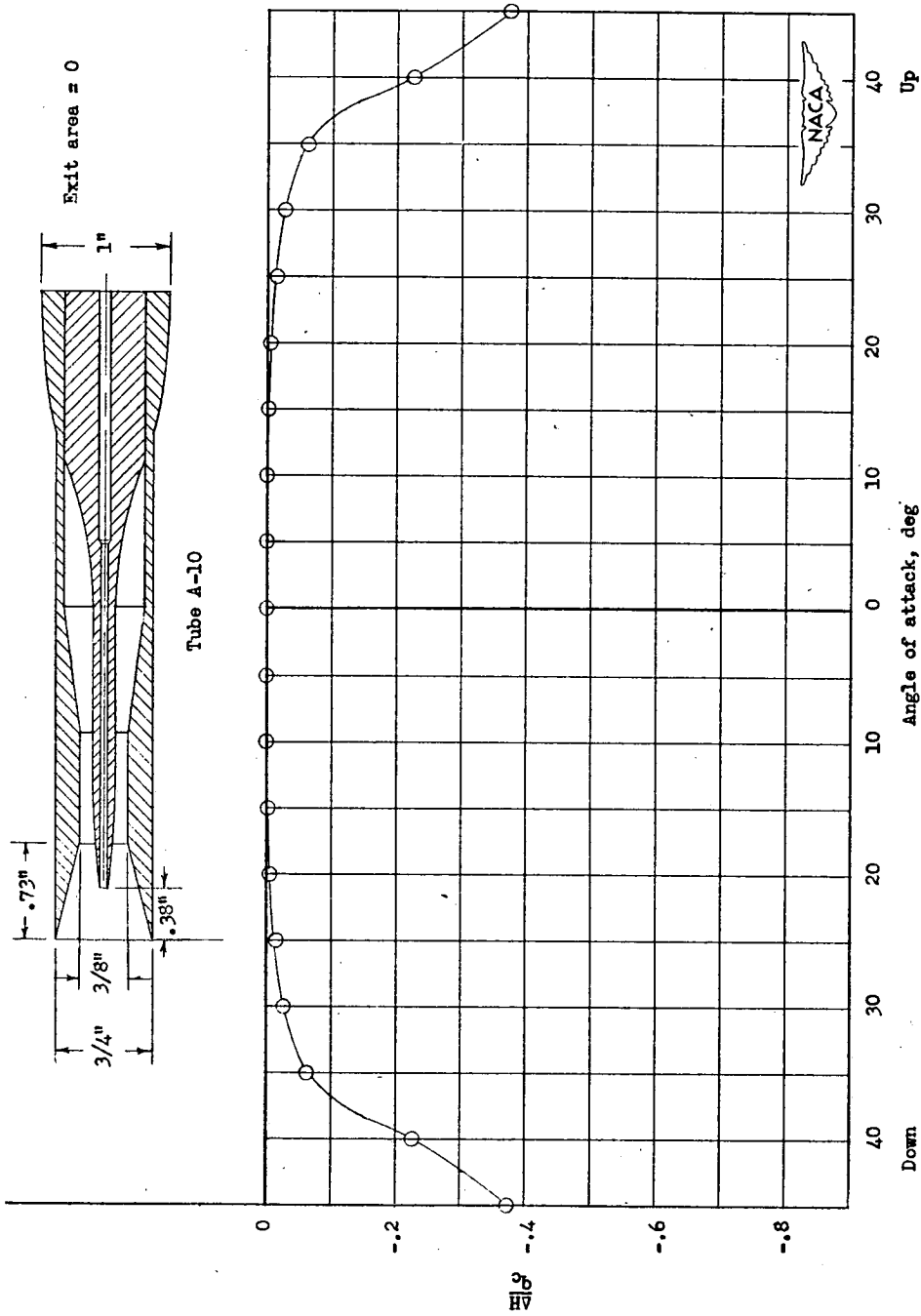


Figure 18.- Variation of total-pressure error with angle of attack. Tube A-10.

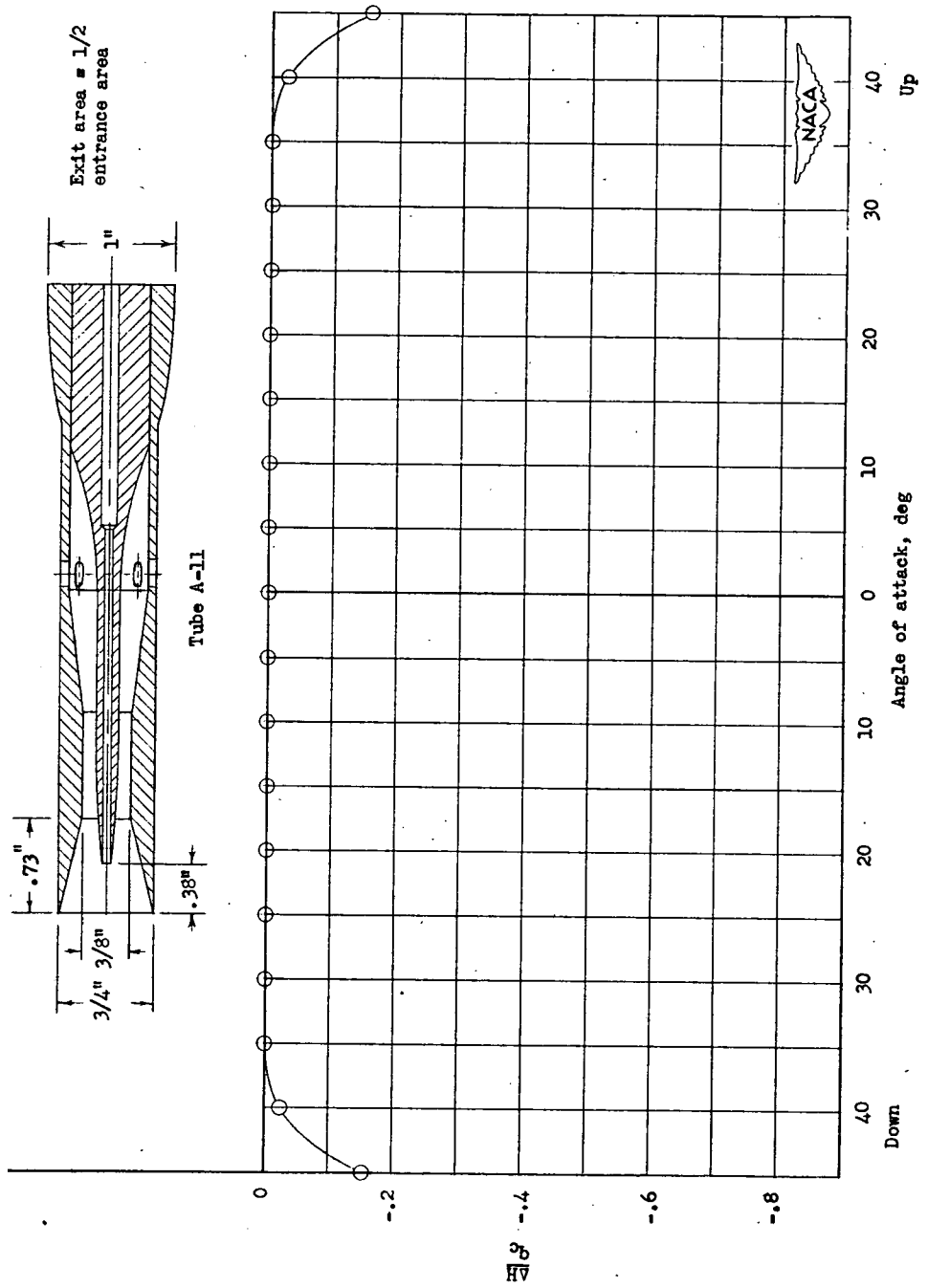


Figure 19.- Variation of total-pressure error with angle of attack. Tube A-11.

6

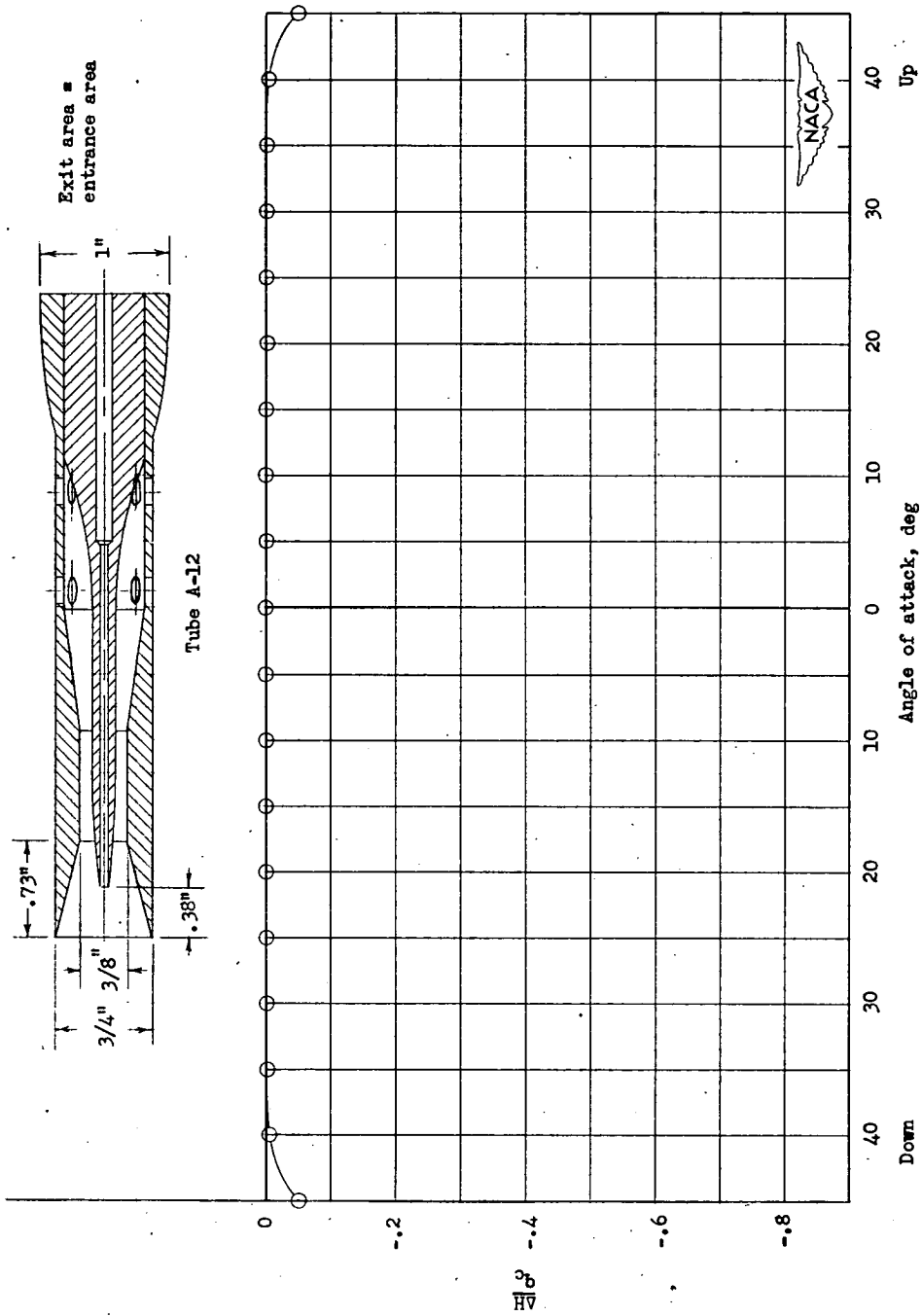


Figure 20.- Variation of total-pressure error with angle of attack.
Tube A-12.

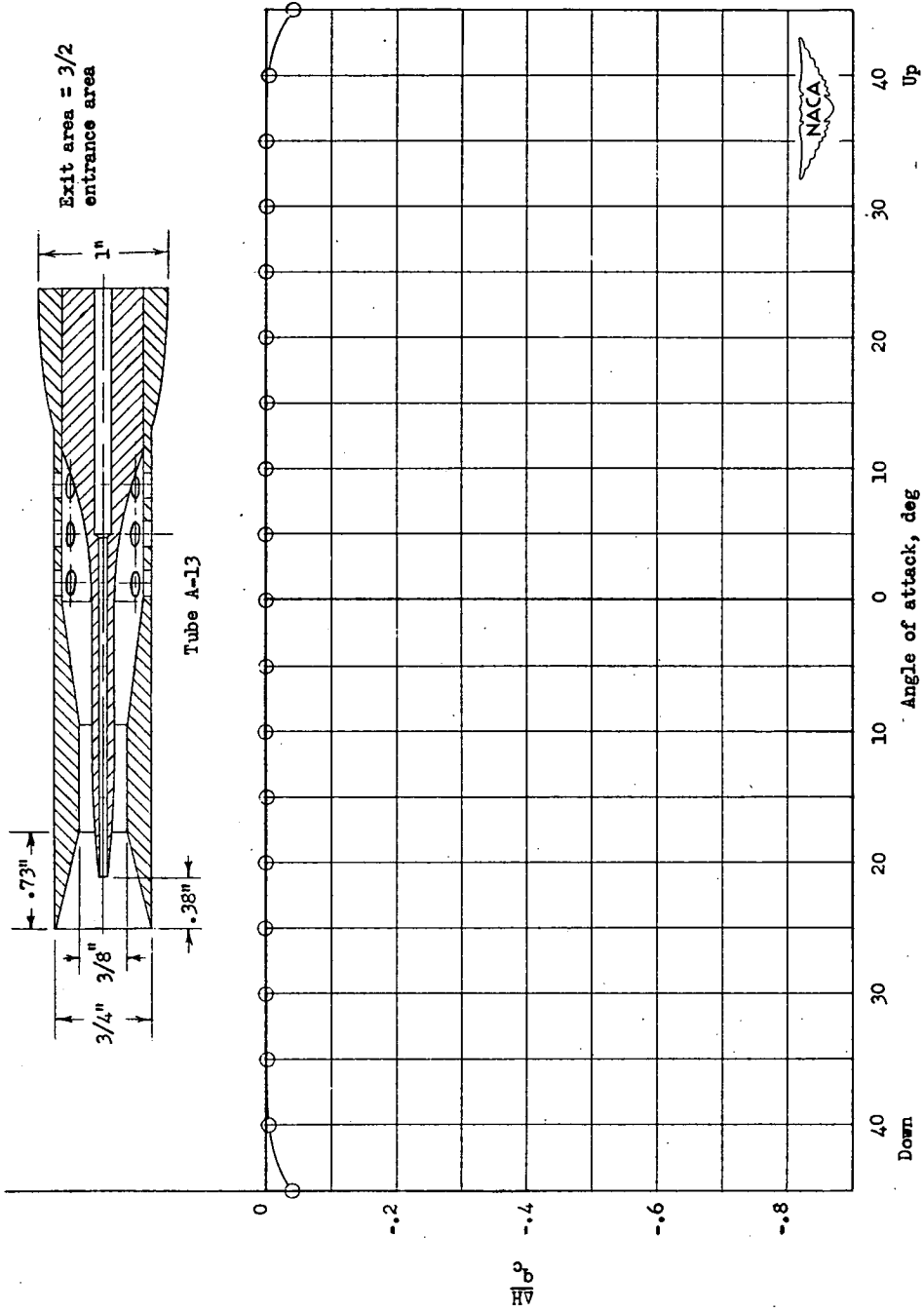


Figure 21.- Variation of total-pressure error with angle of attack.
Tube A-13.

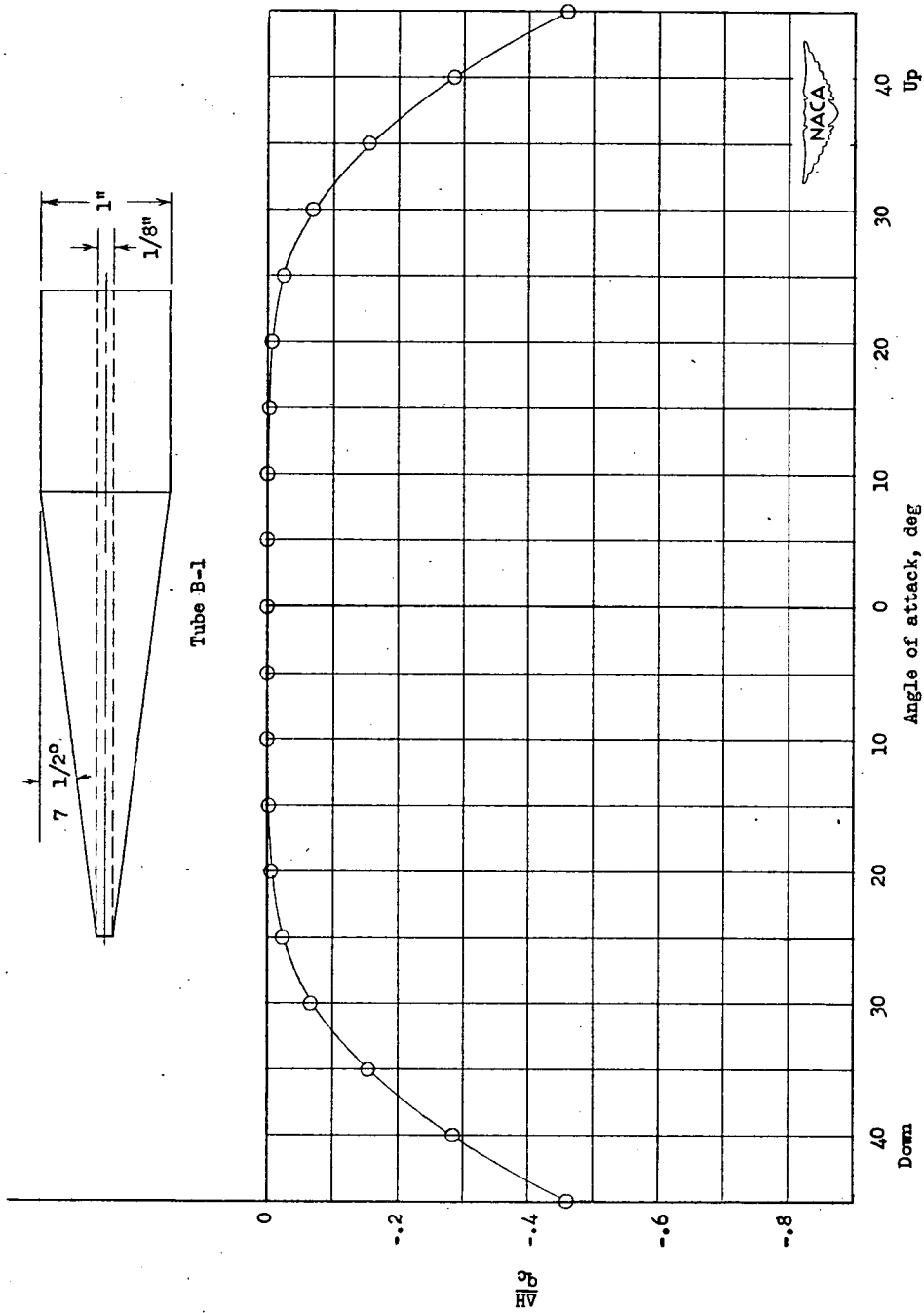


Figure 22.- Variation of total-pressure error with angle of attack.
Tube B-1.

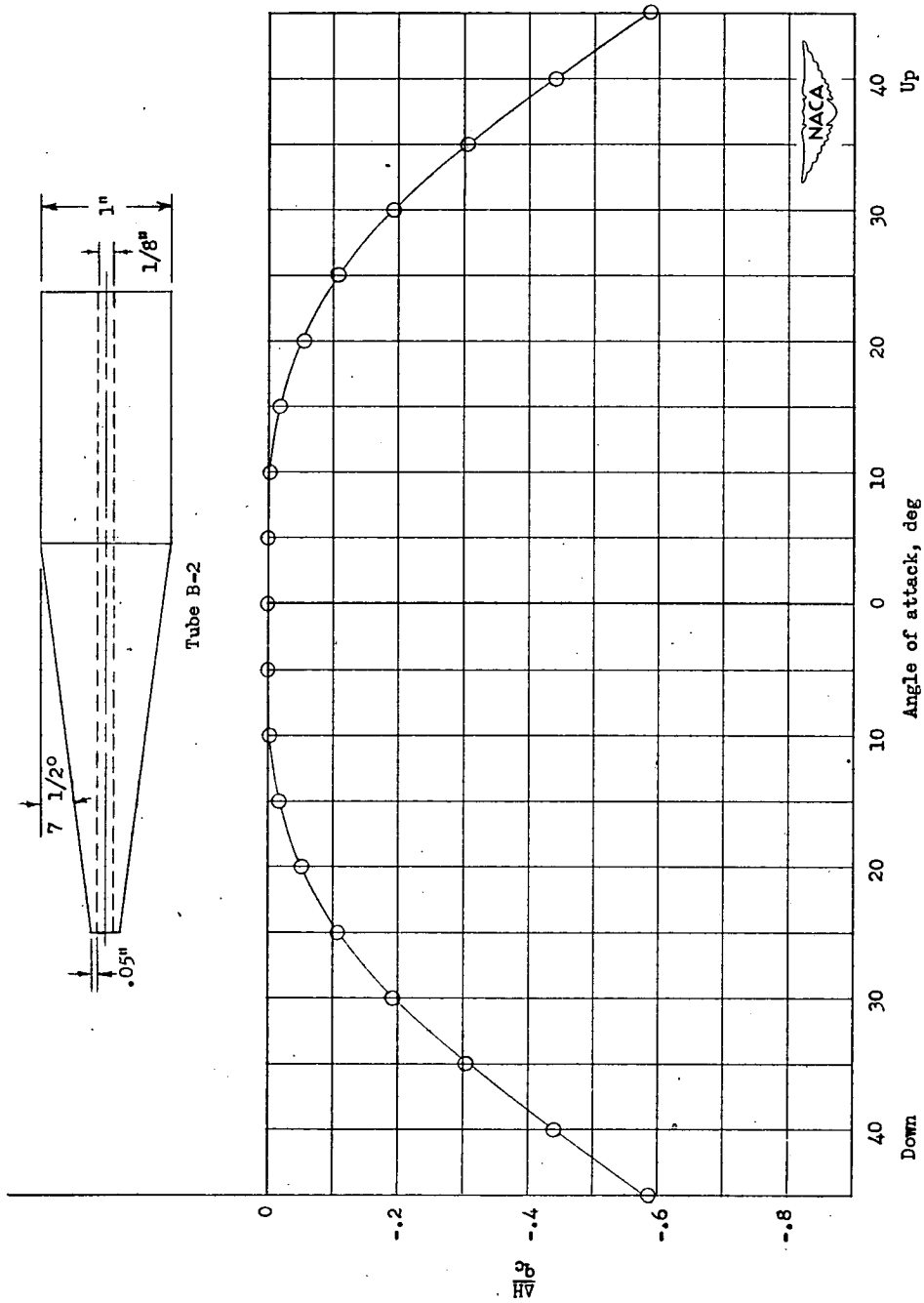


Figure 23.- Variation of total-pressure error with angle of attack. Tube B-2.



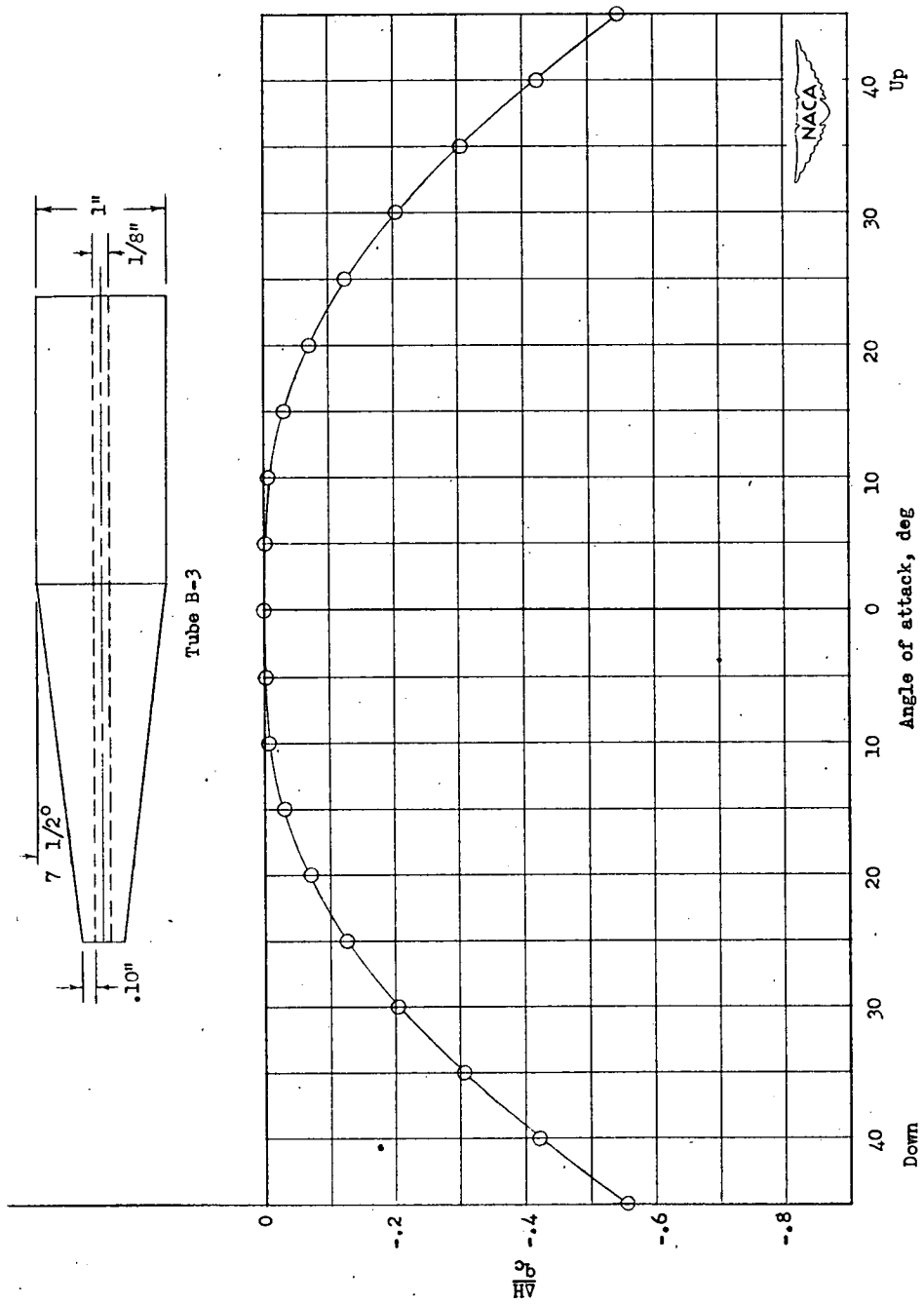


Figure 24.- Variation of total-pressure error with angle of attack.
Tube B-3.

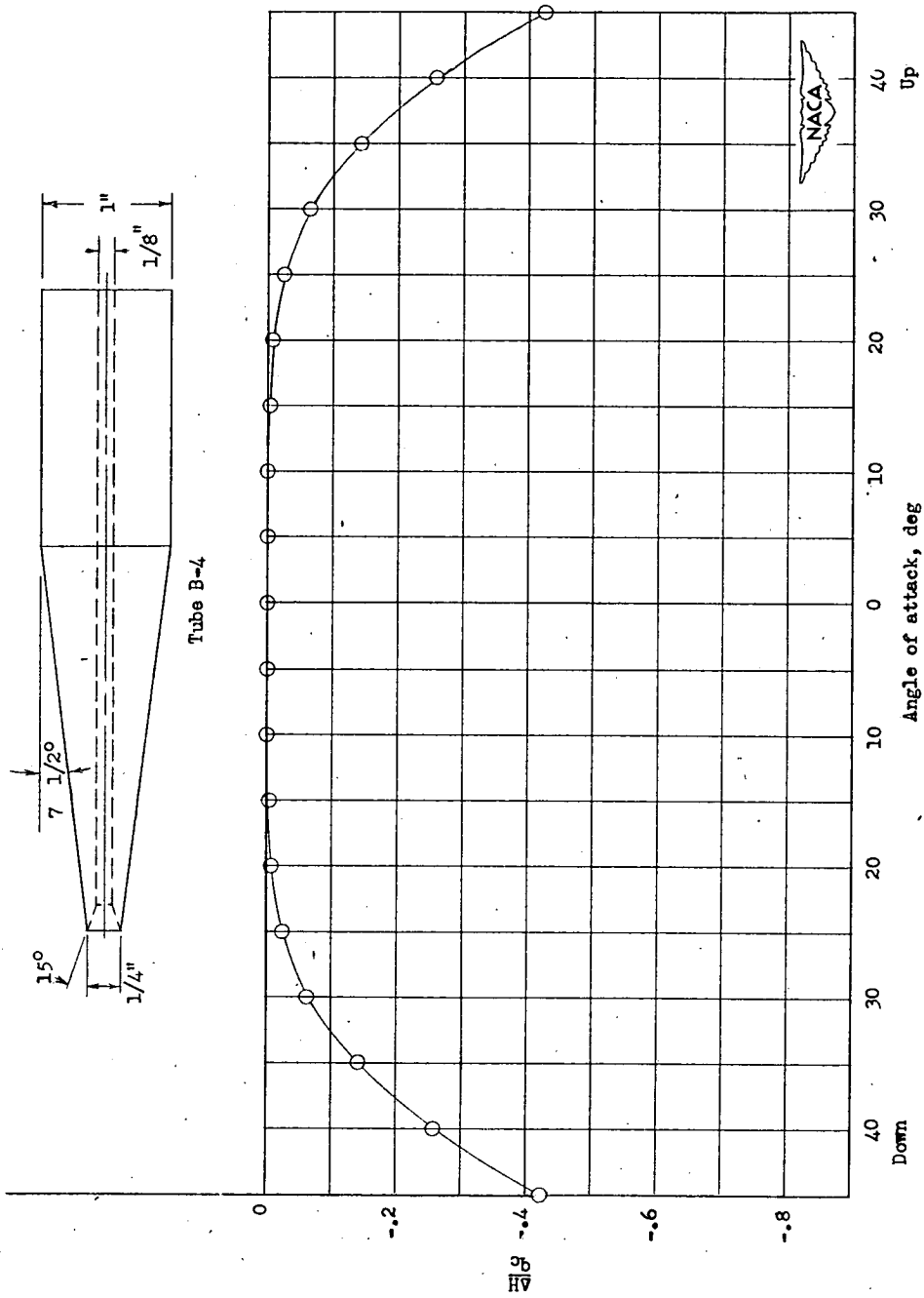


Figure 25.- Variation of total-pressure error with angle of attack.
Tube B-4.

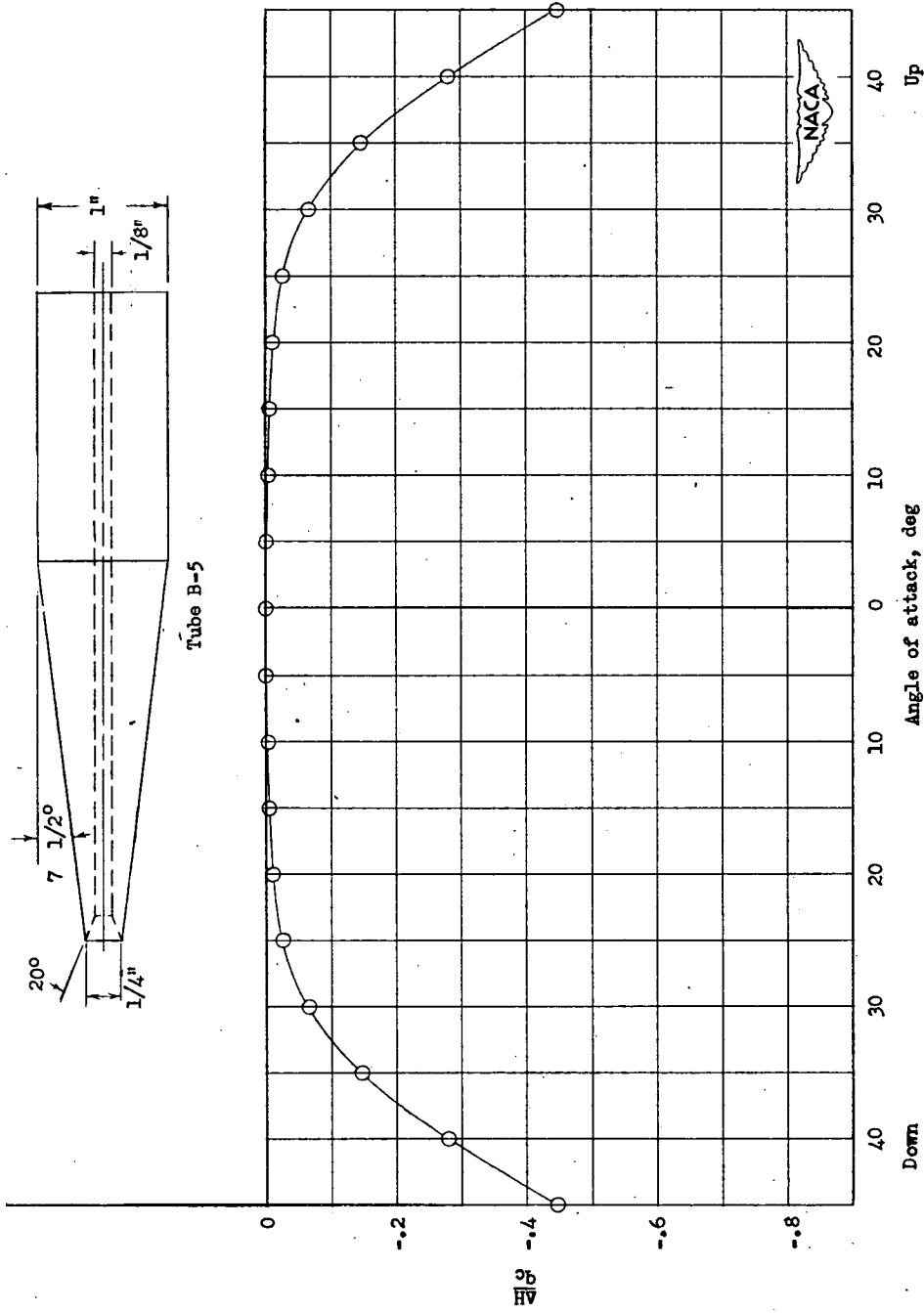


Figure 26.- Variation of total-pressure error with angle of attack. Tube B-5.

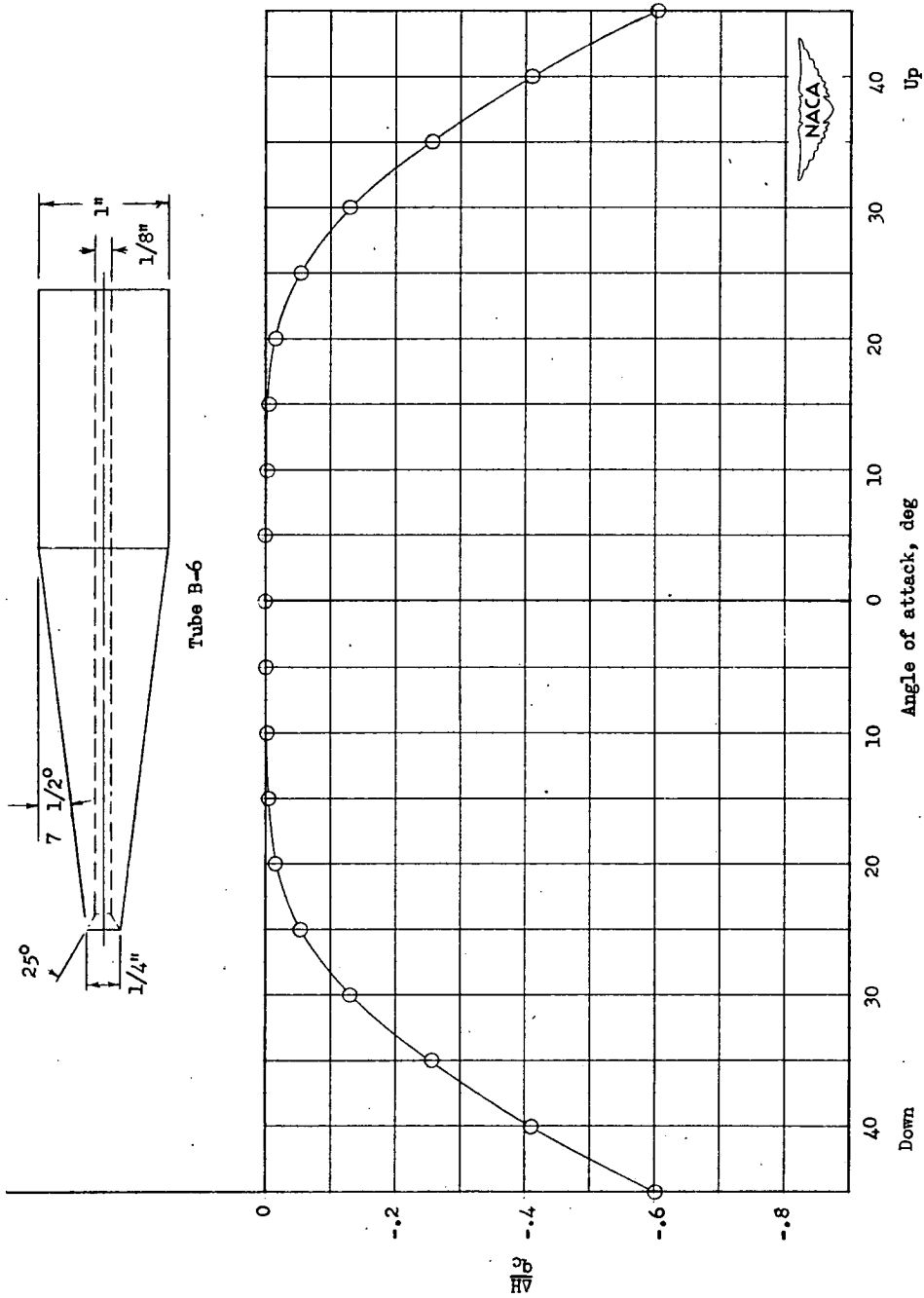


Figure 27.- Variation of total-pressure error with angle of attack.
Tube B-6.

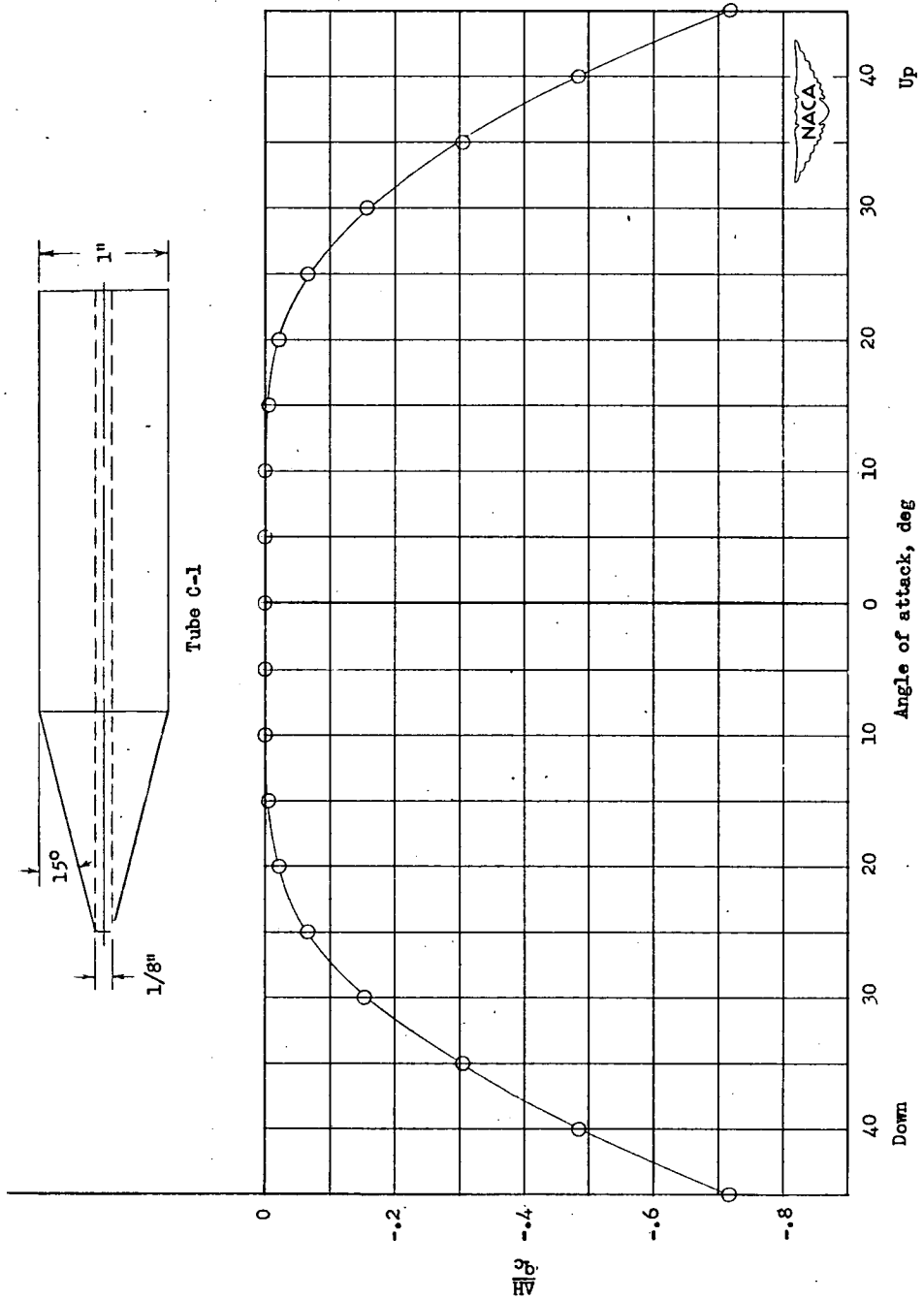


Figure 28.- Variation of total-pressure error with angle of attack.
Tube C-1.

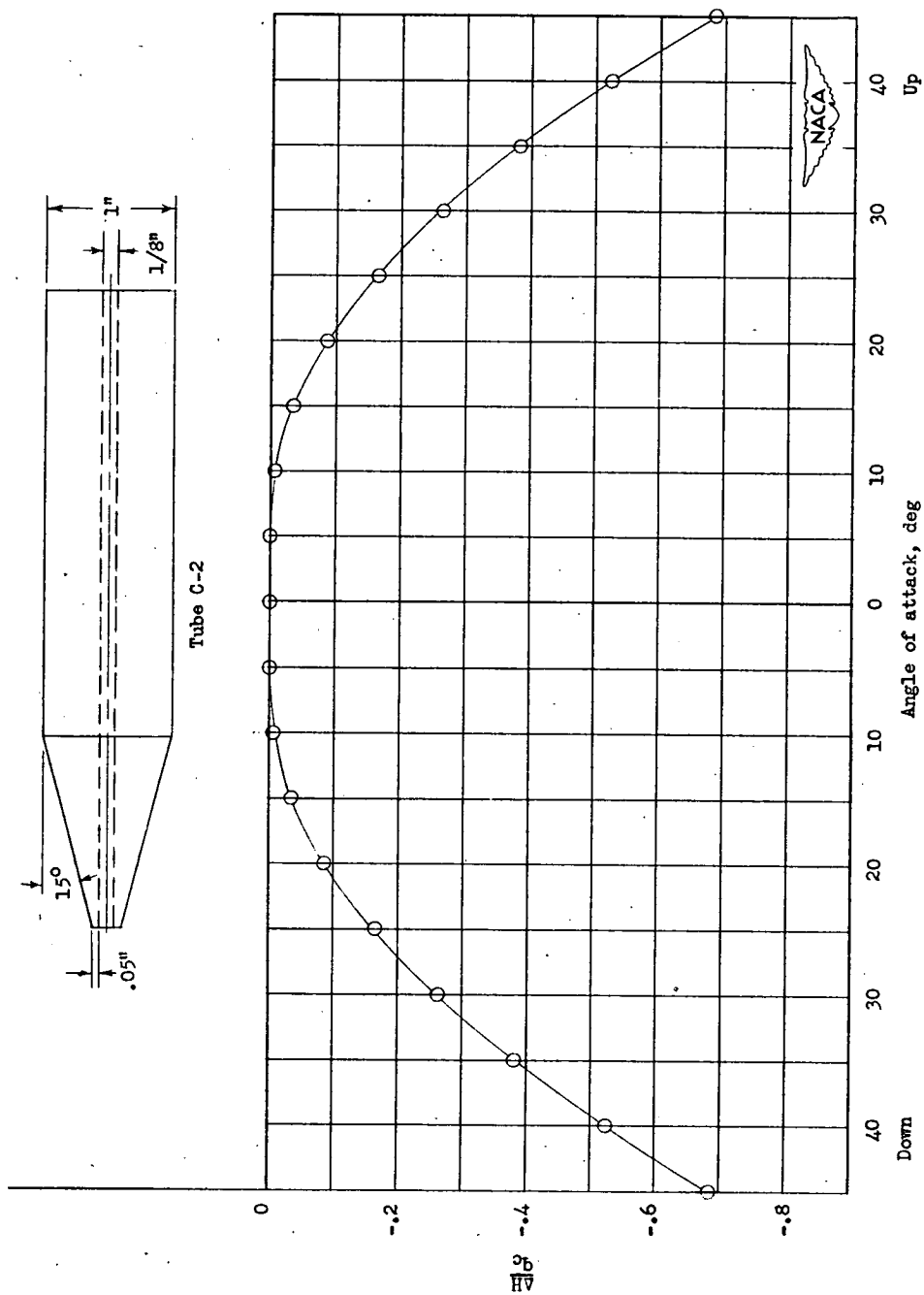


Figure 29.- Variation of total-pressure error with angle of attack.
Tube C-2.

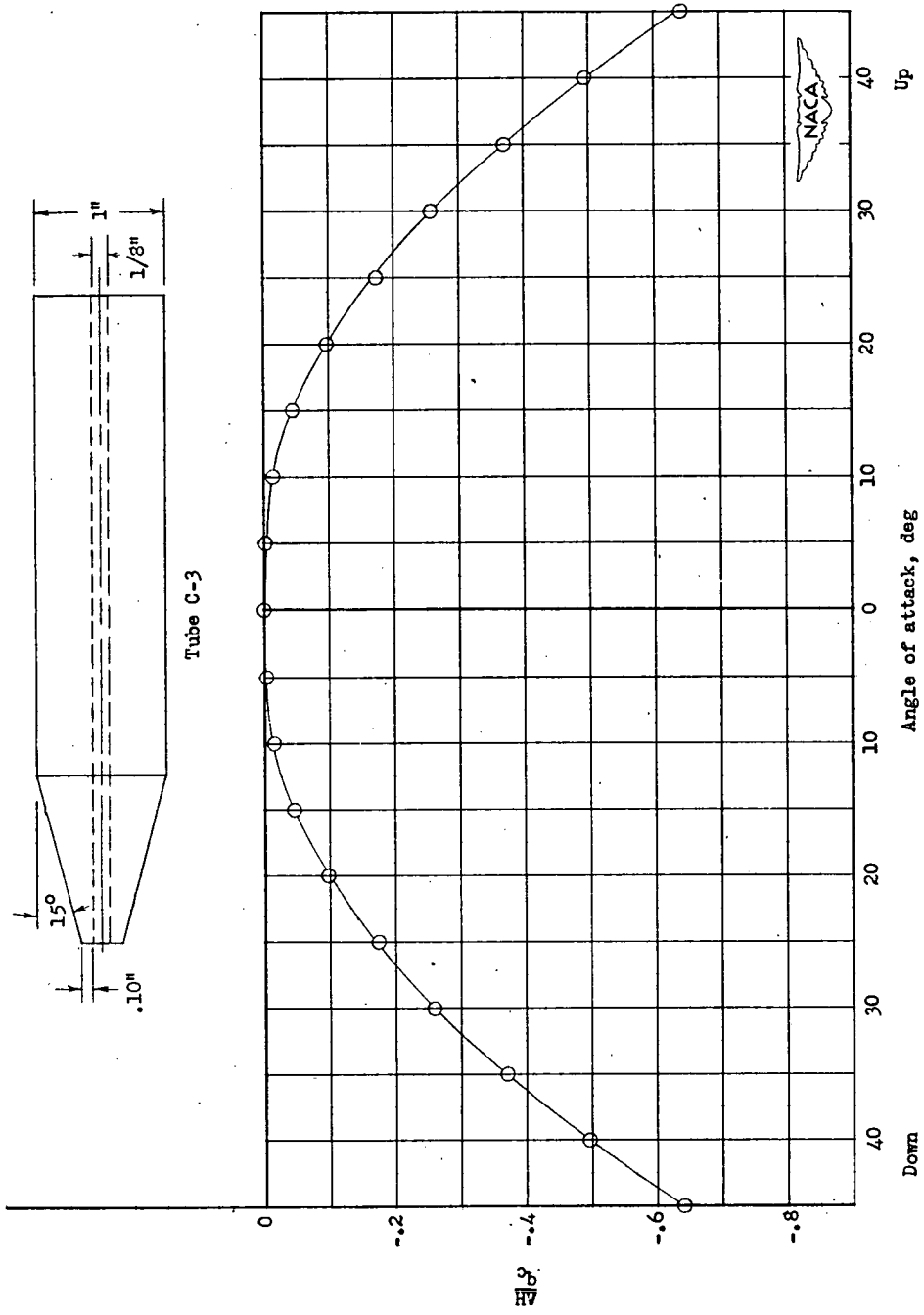


Figure 30.- Variation of total-pressure error with angle of attack. Tube C-3.

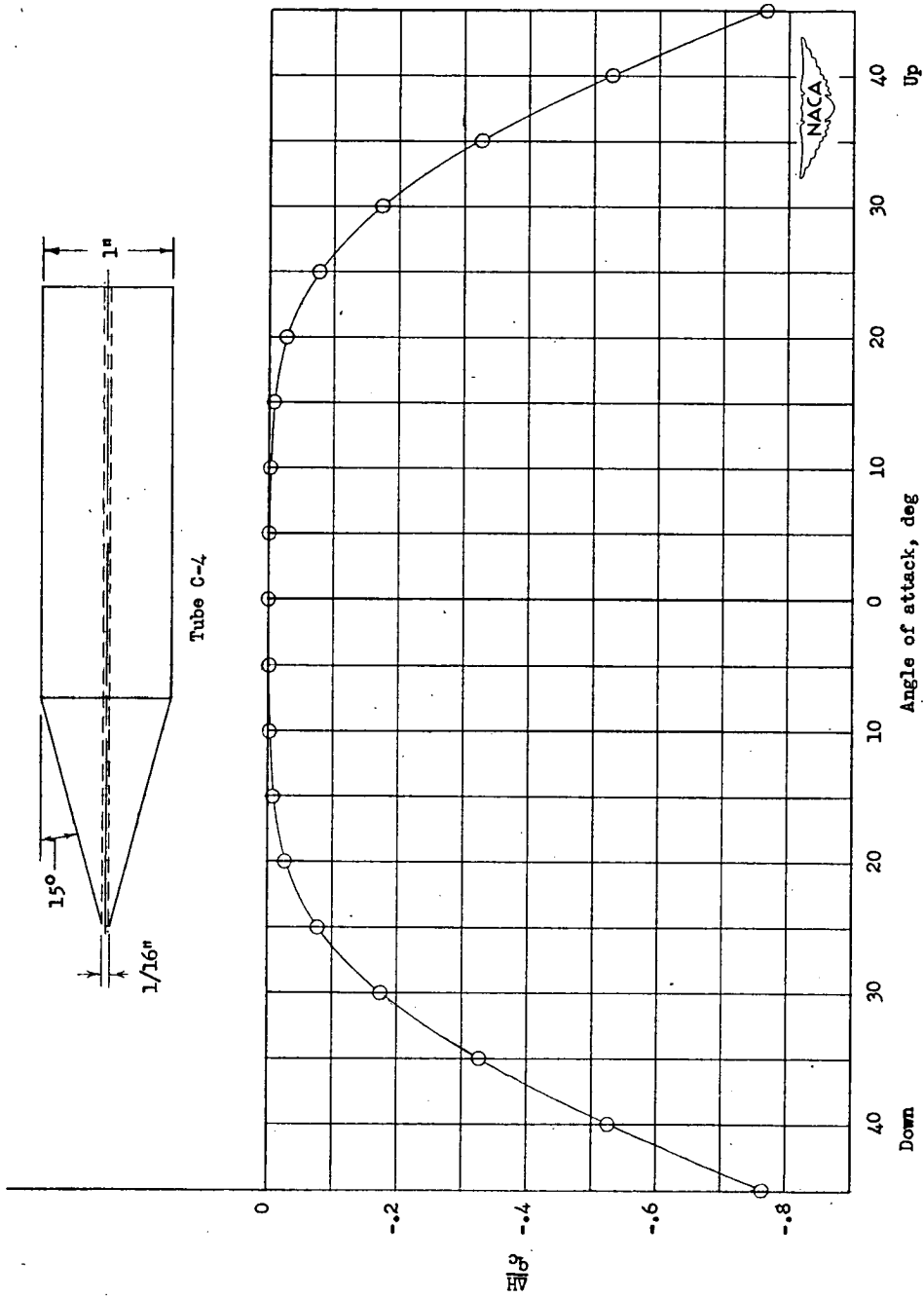


Figure 31.- Variation of total-pressure error with angle of attack.
Tube C-4.

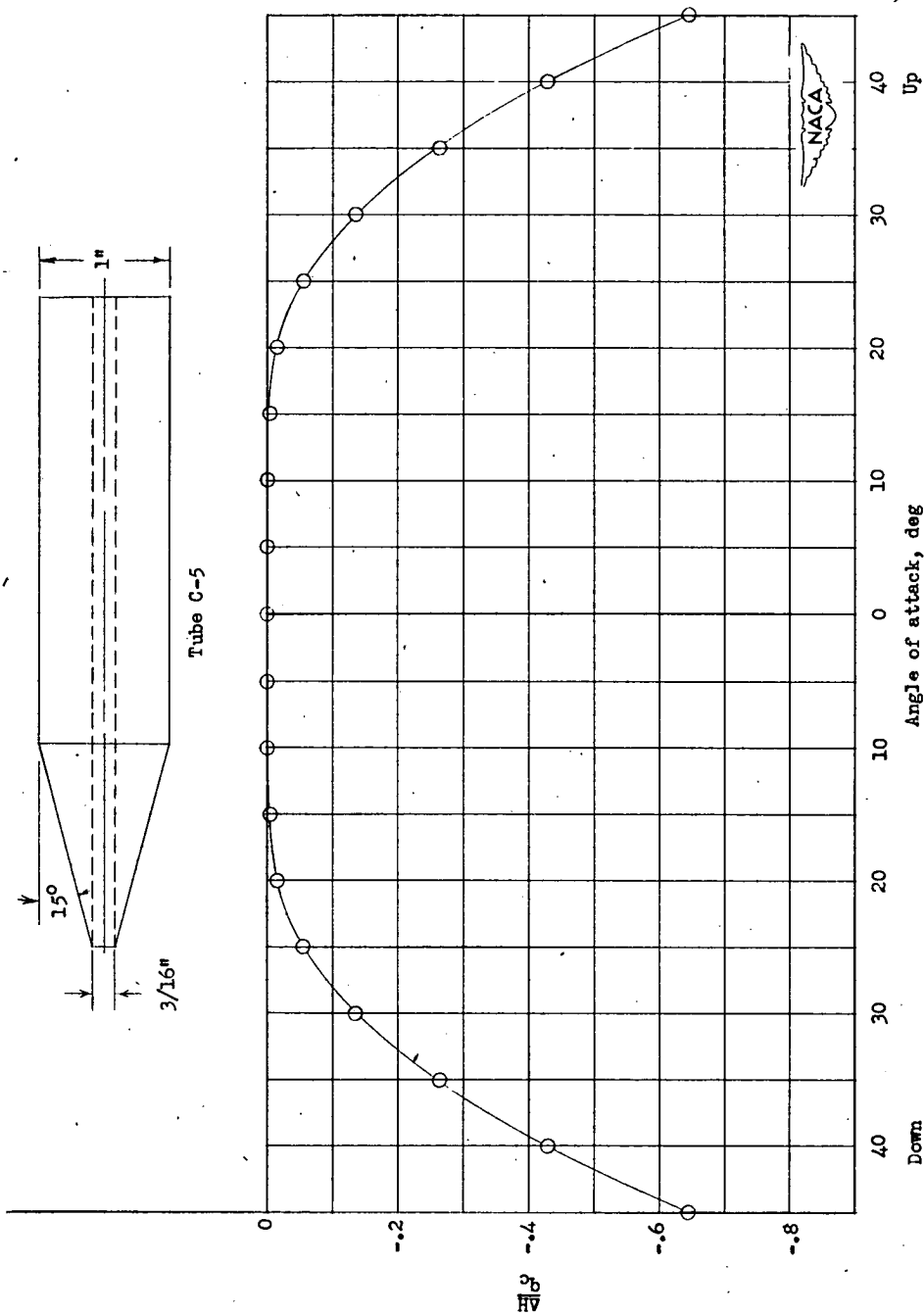


Figure 32.- Variation of total-pressure error with angle of attack.
Tube C-5.

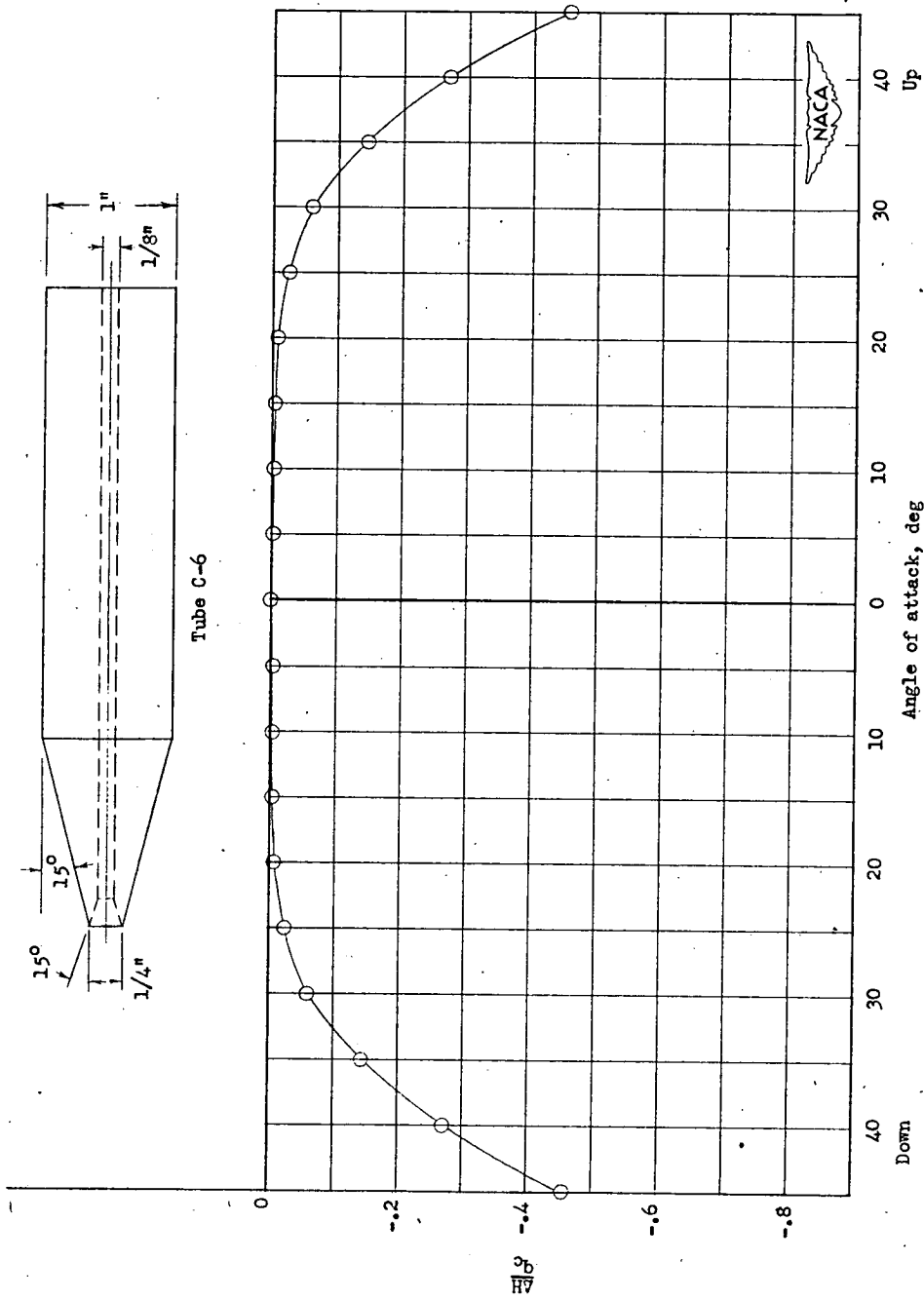


Figure 33.- Variation of total-pressure error with angle of attack.
Tube C-6.

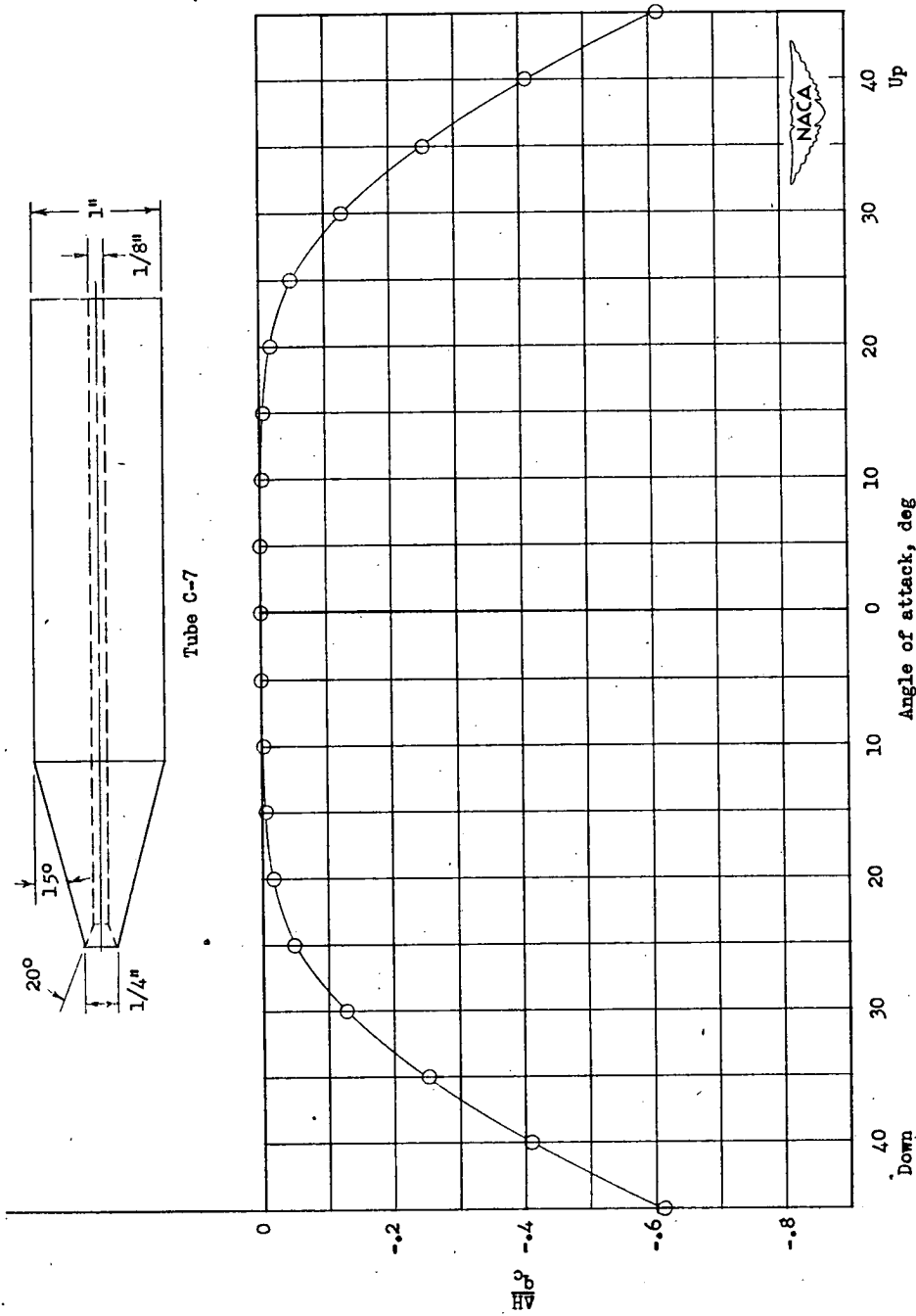


Figure 34.- Variation of total-pressure error with angle of attack.
Tube C-7.

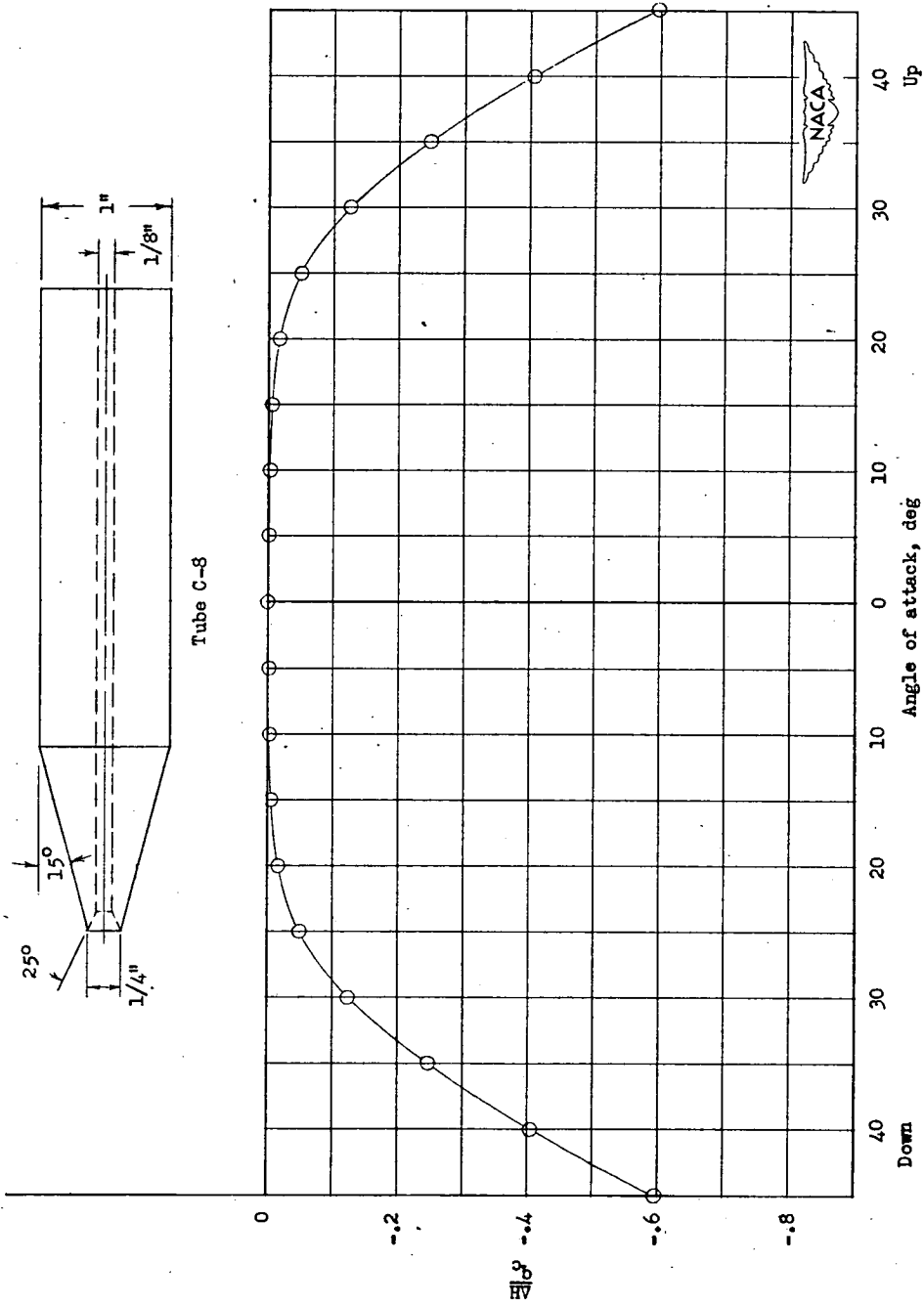


Figure 35.- Variation of total-pressure error with angle of attack.
Tube C-8:

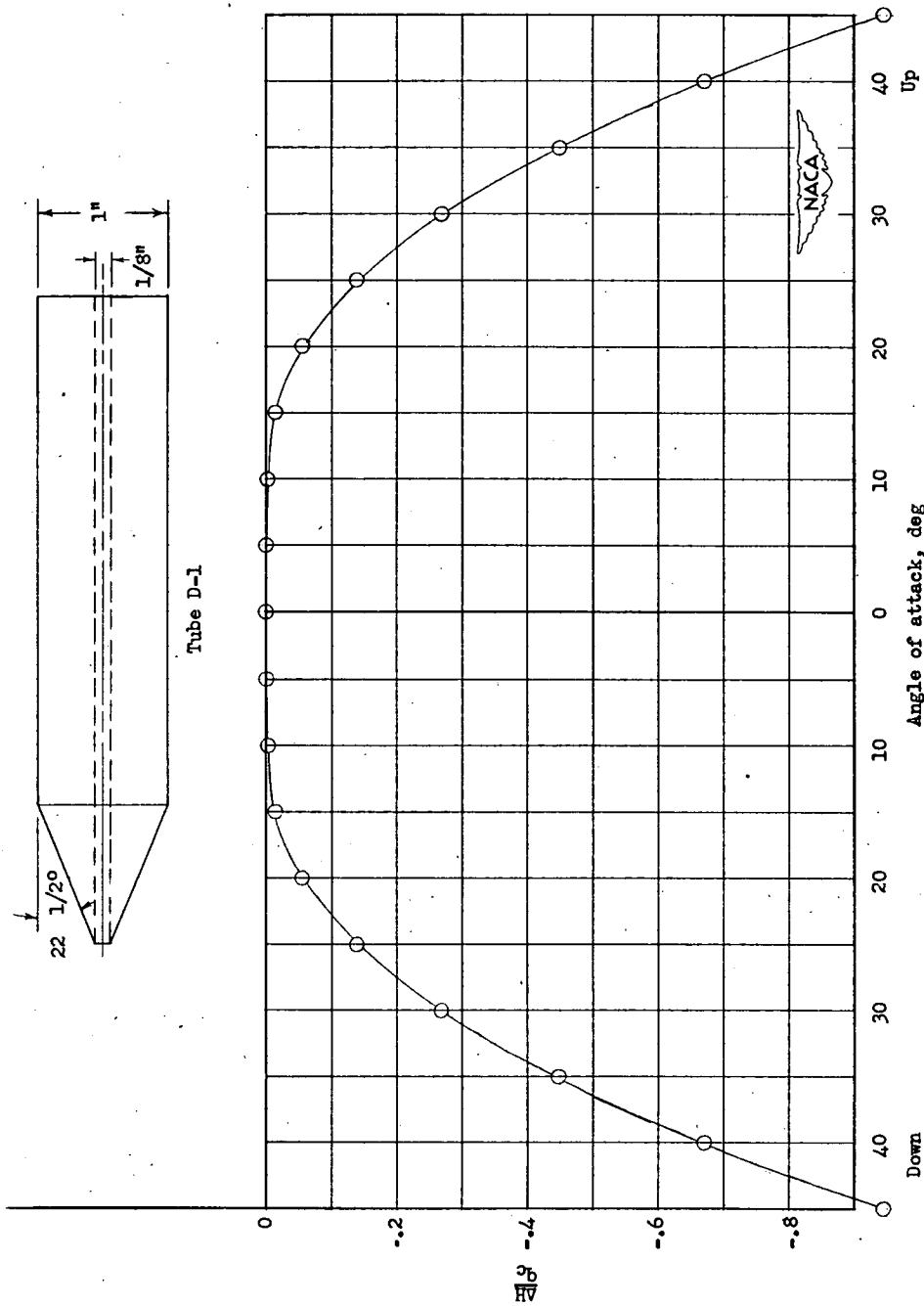


Figure 36.- Variation of total-pressure error with angle of attack. Tube D-1.

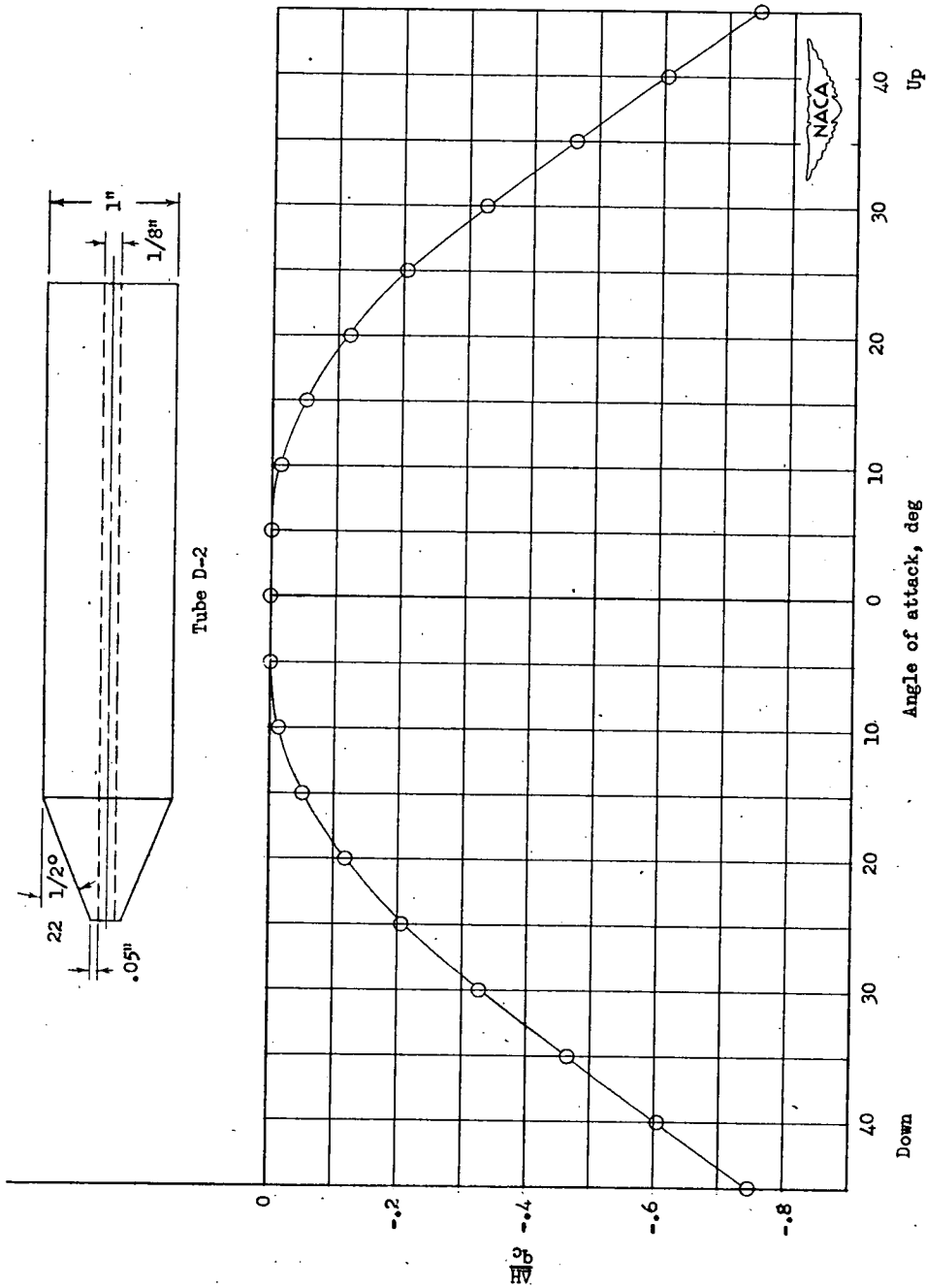


Figure 37.- Variation of total-pressure error with angle of attack. Tube D-2.

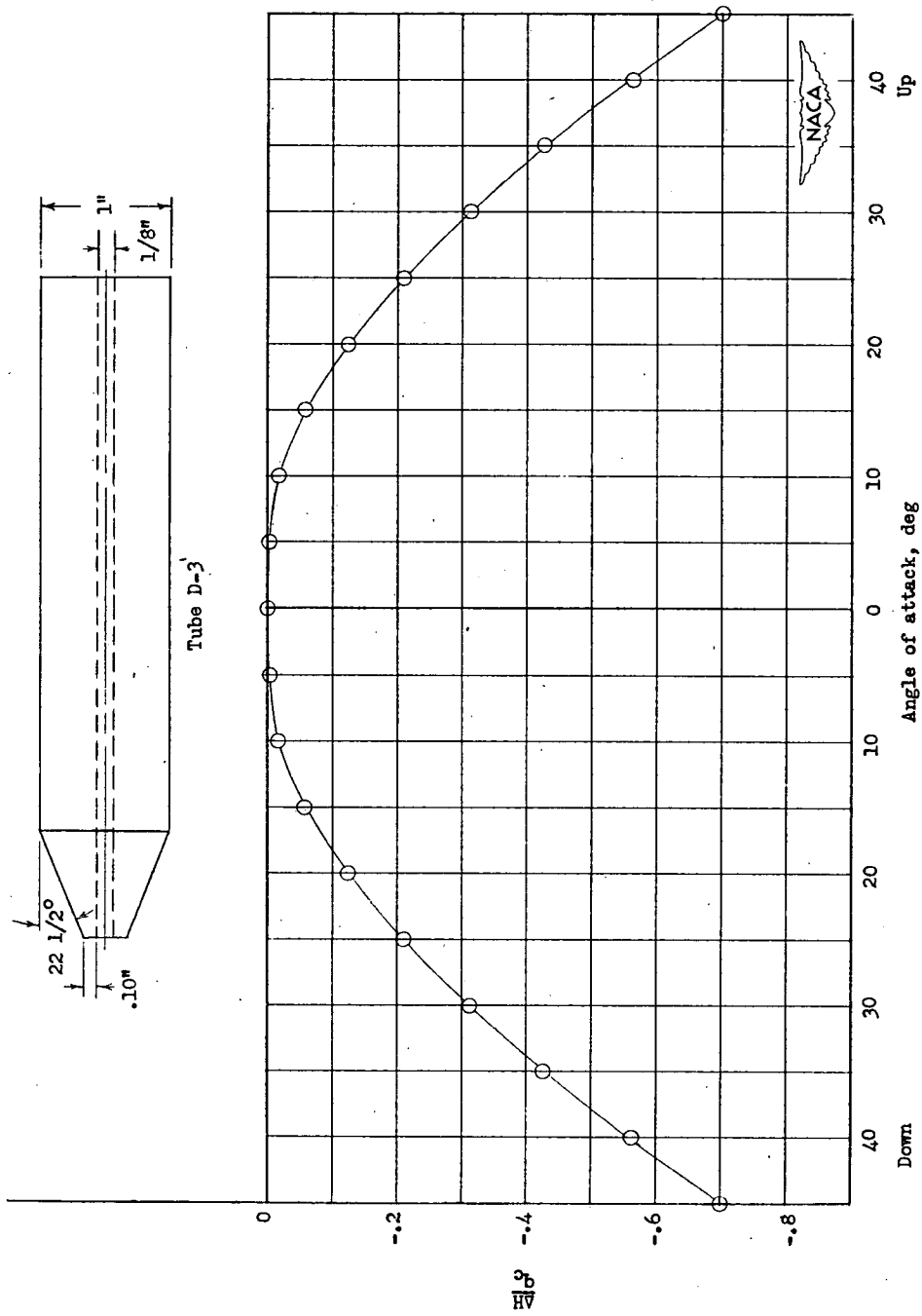


Figure 38.- Variation of total-pressure error with angle of attack.
Tube D-3.

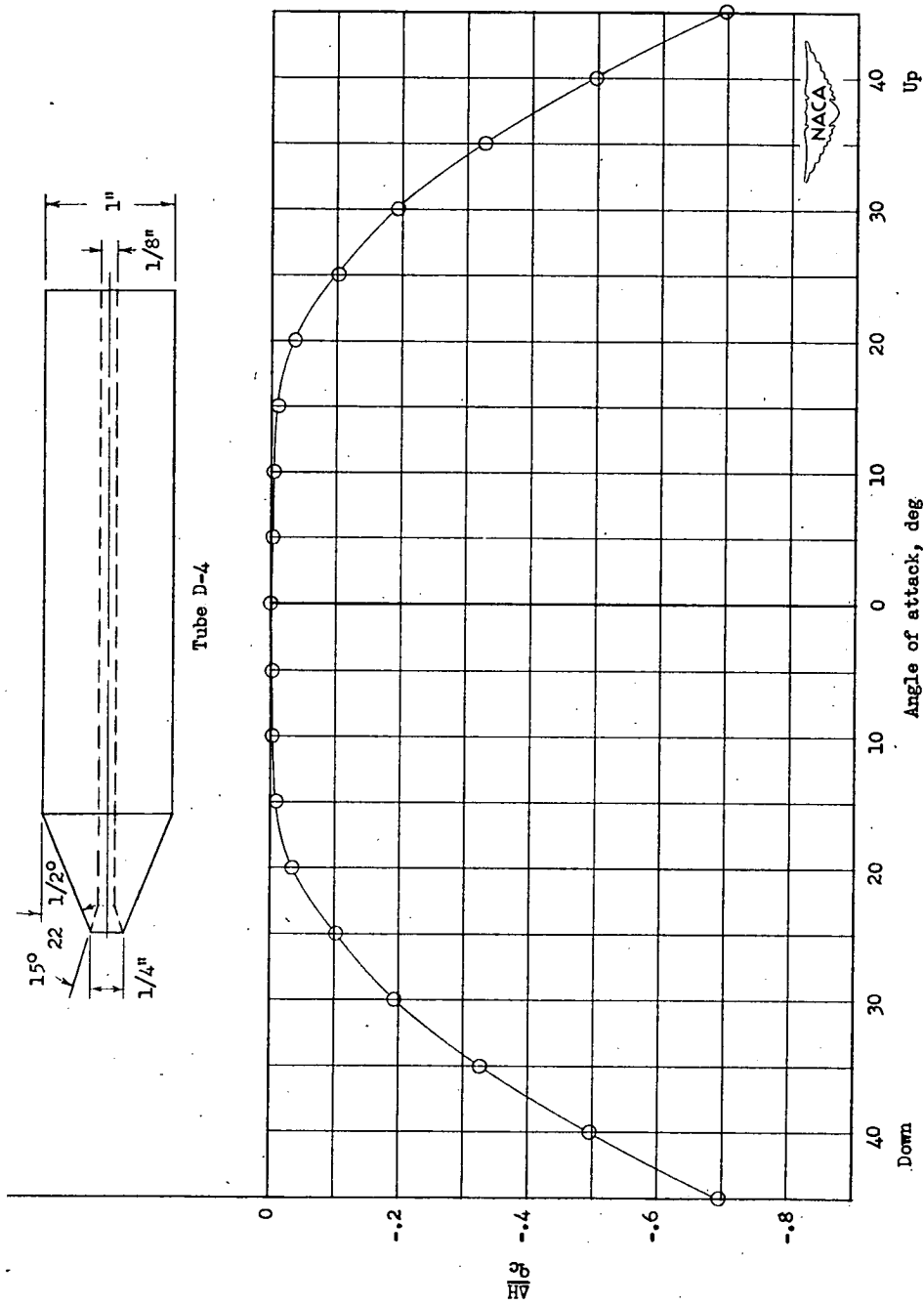


Figure 39.- Variation of total-pressure error with angle of attack.
Tube D-4.

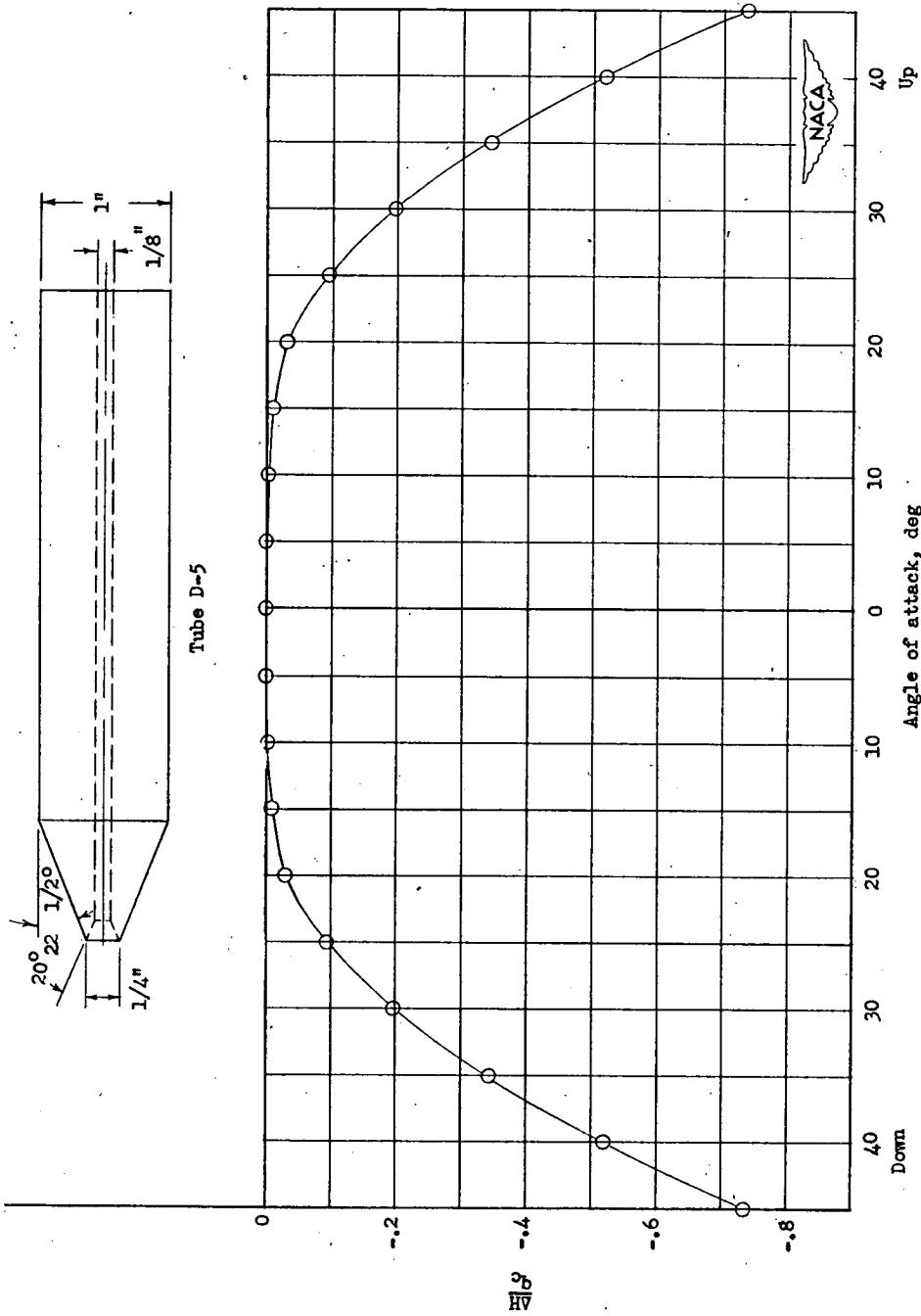


Figure 40.- Variation of total-pressure error with angle of attack.
Tube D-5.

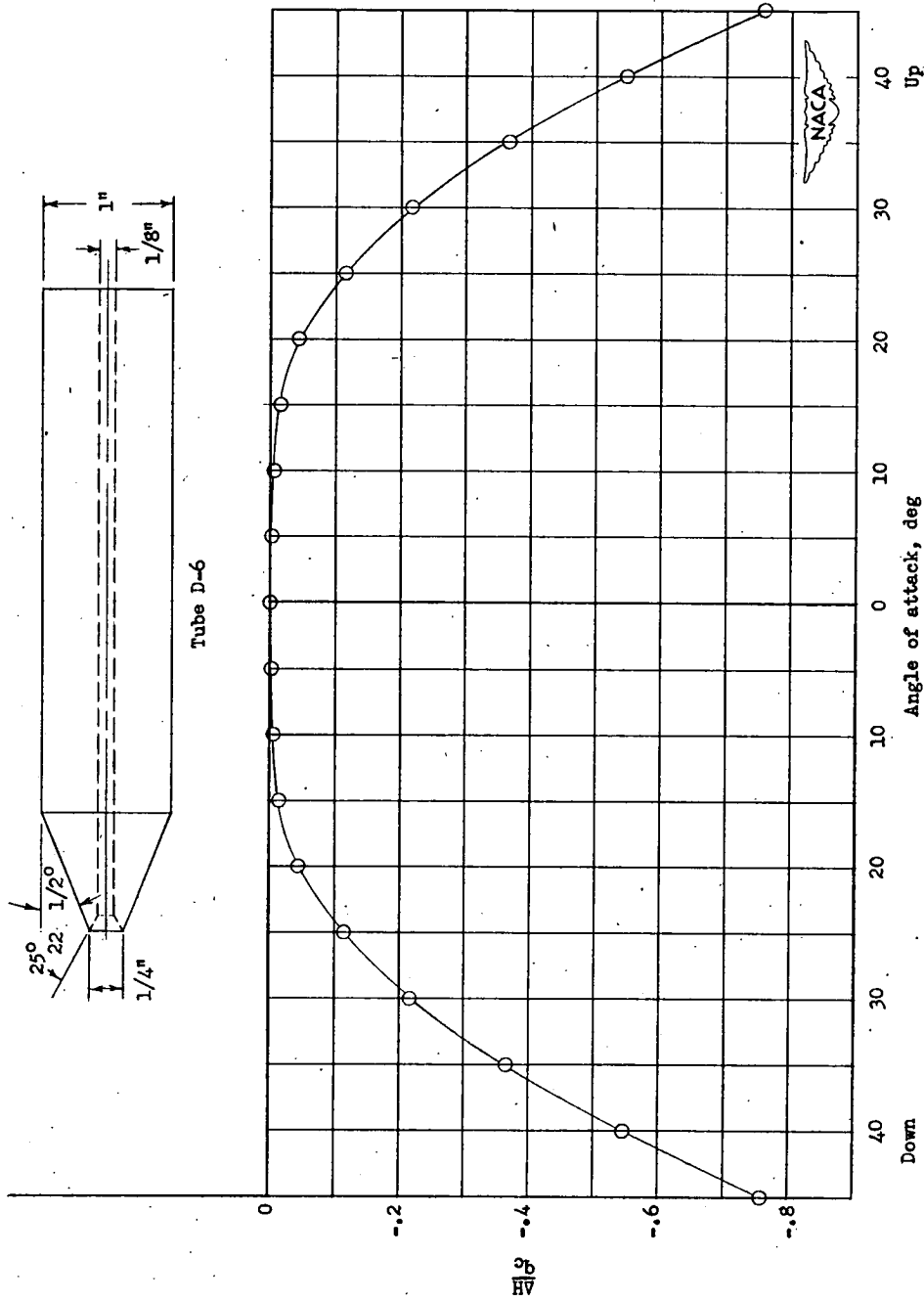


Figure 41.- Variation of total-pressure error with angle of attack.
Tube D-6.

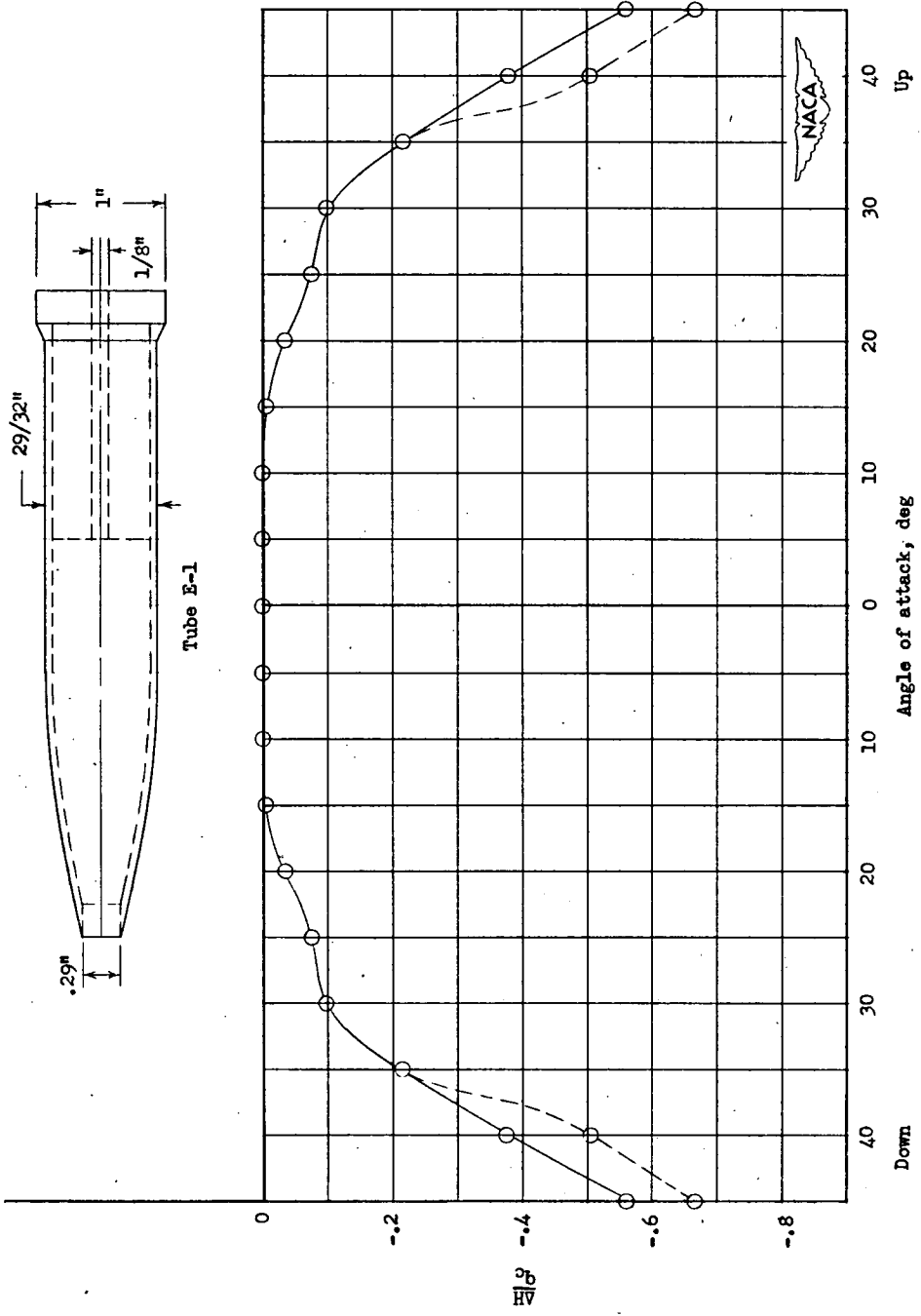


Figure 42.- Variation of total-pressure error with angle of attack. Tube E-1.

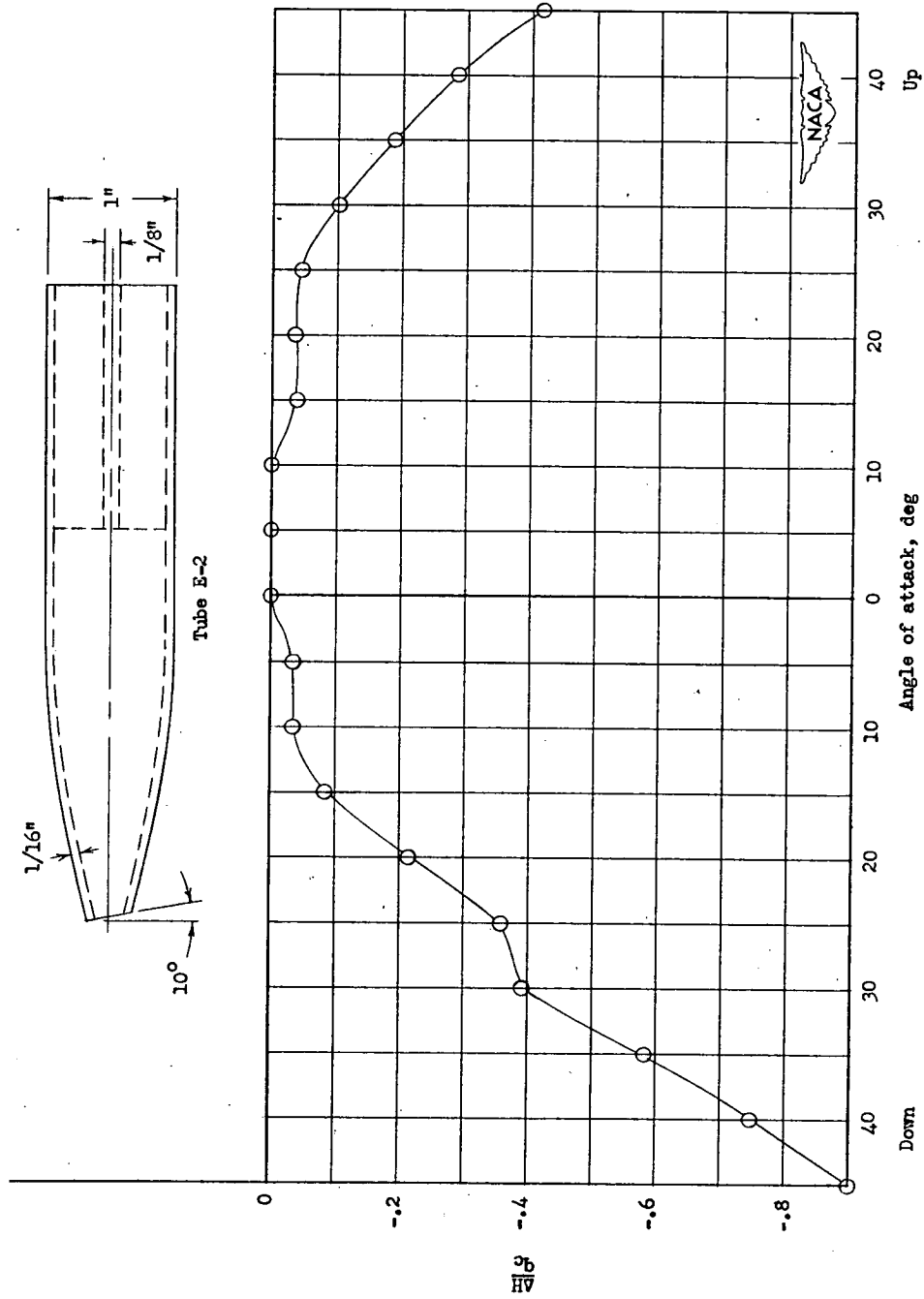


Figure 43.- Variation of total-pressure error with angle of attack.
Tube E-2.

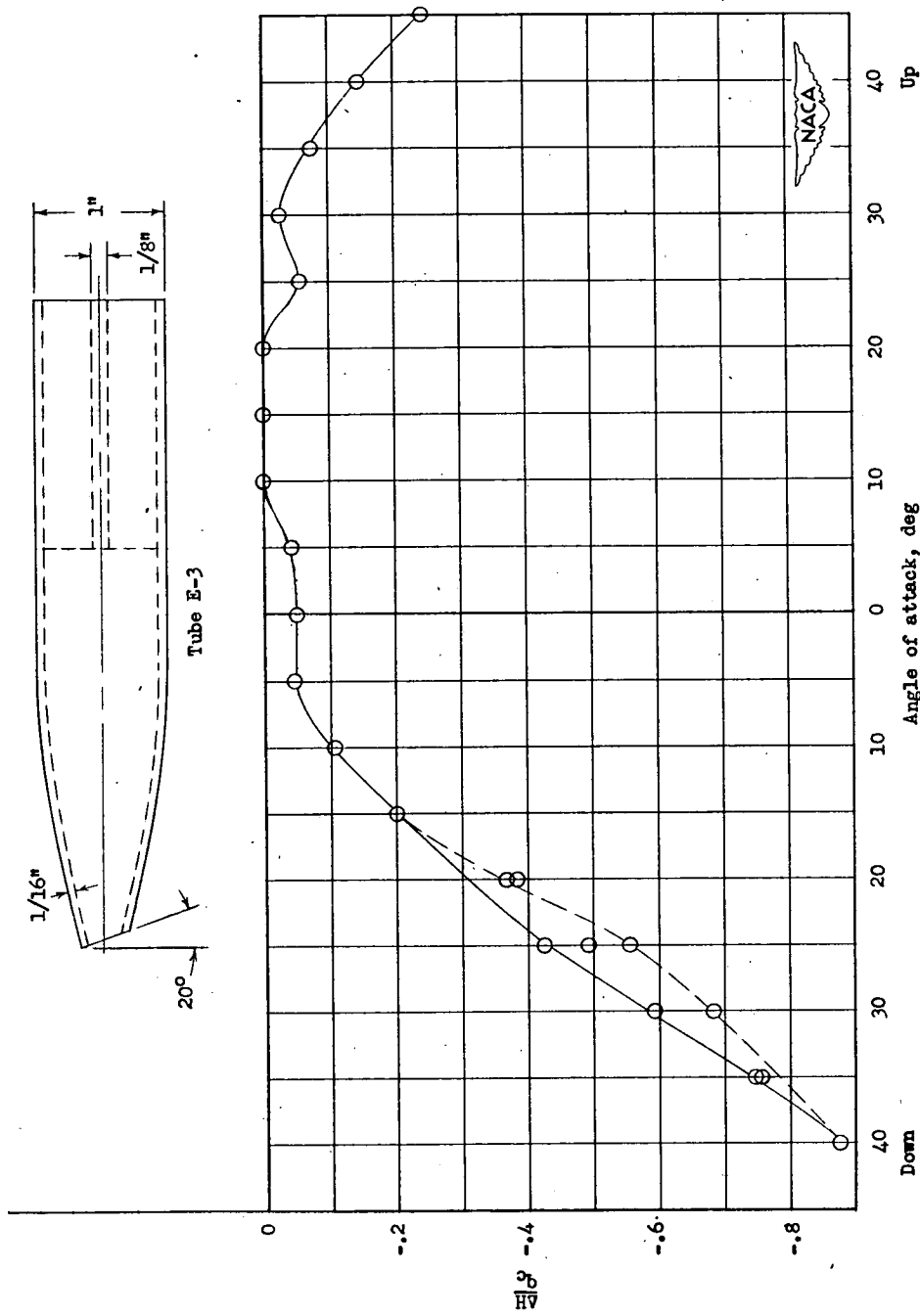


Figure 44.- Variation of total-pressure error with angle of attack.
Tube E-3.

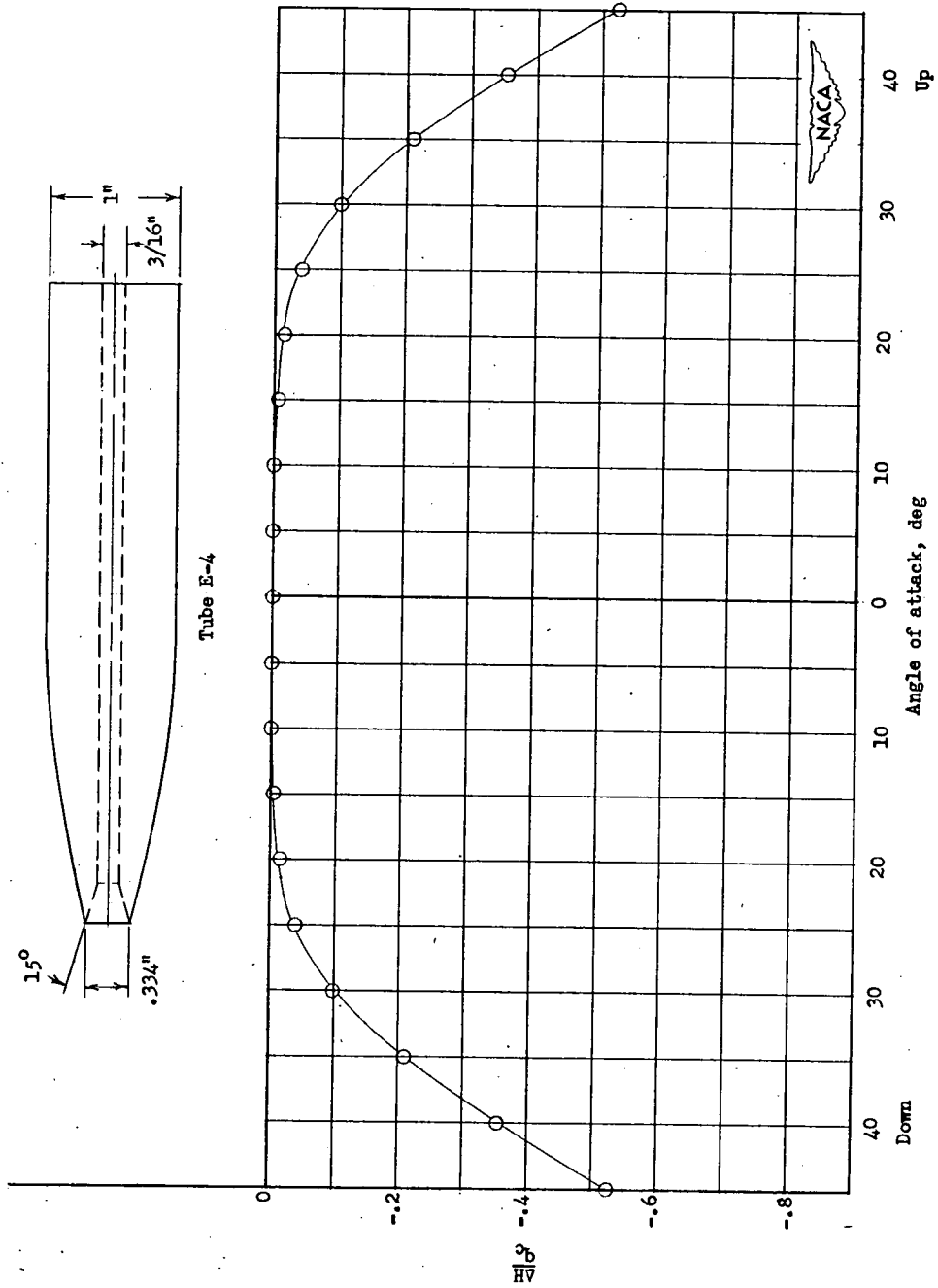


Figure 45.- Variation of total-pressure error with angle of attack.
Tube E-4.

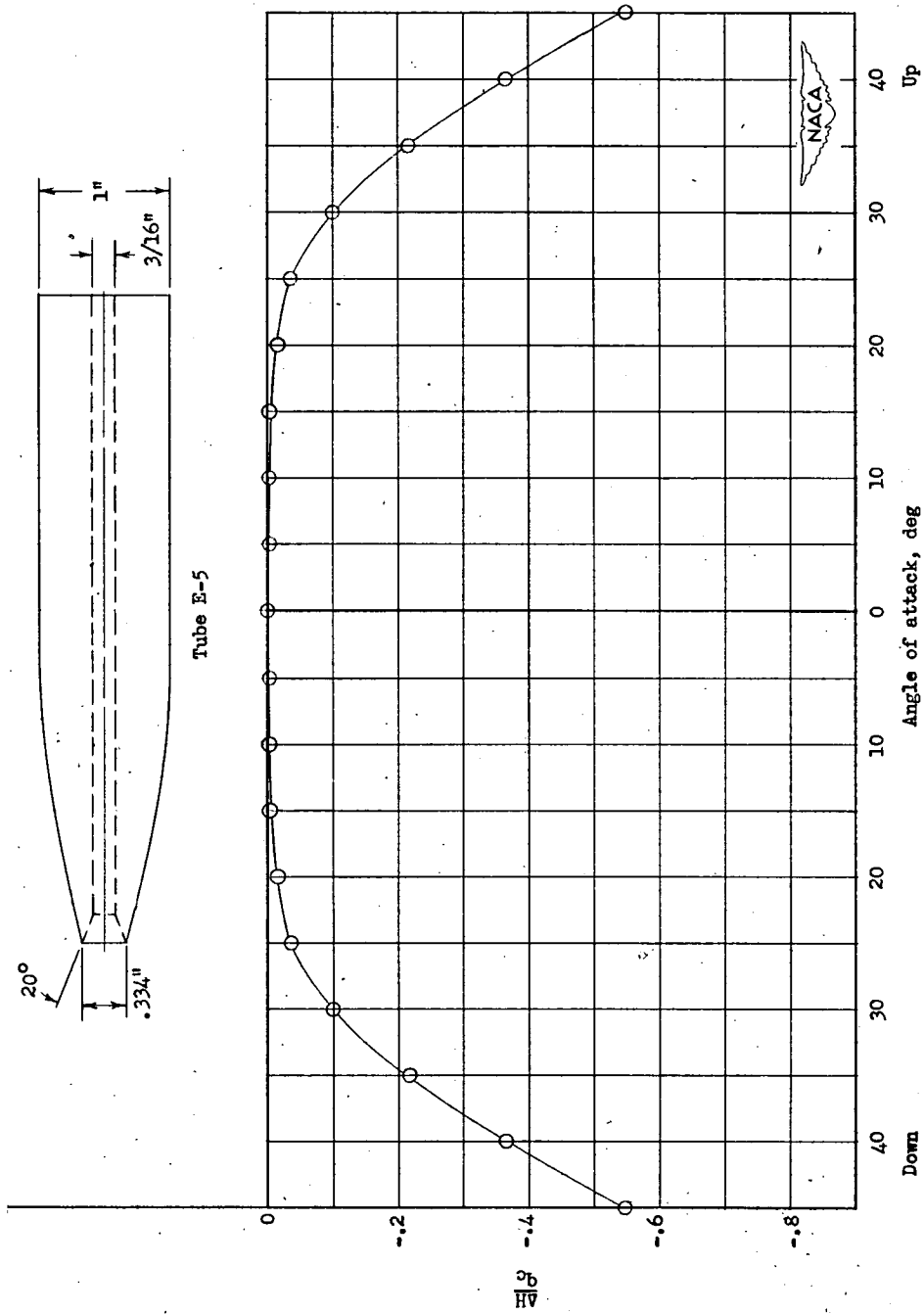


Figure 46.- Variation of total-pressure error with angle of attack. Tube E-5.

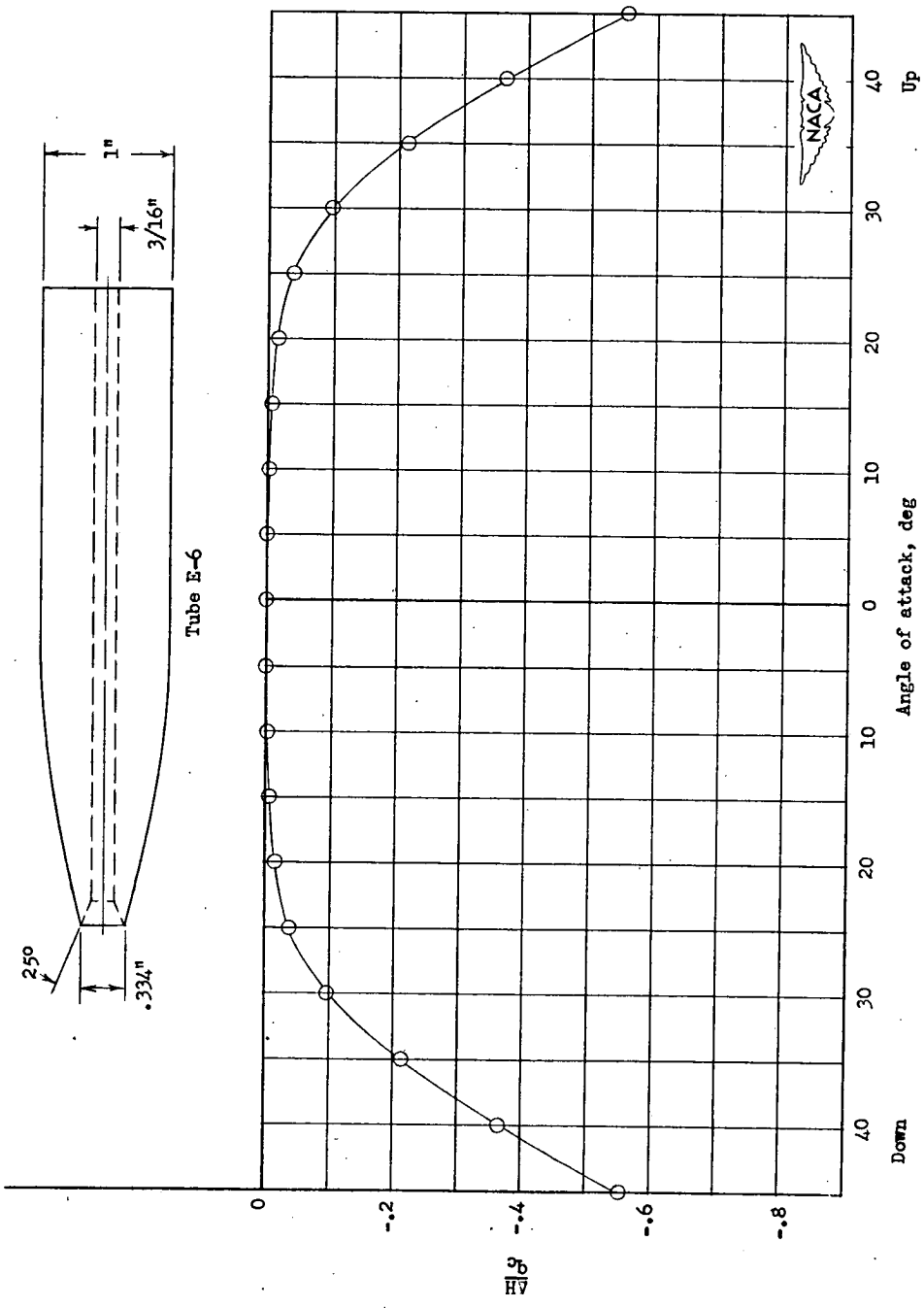


Figure 47.- Variation of total-pressure error with angle of attack.
Tube E-6.